Thesis for the Degree of Doctor of Philosophy in Natural Science, Specialization in Chemistry

Water Condensation and Freezing in the Atmosphere: Exploring Deliquescence and Ice Nucleation

Dimitri Castarède

UNIVERSITY OF GOTHENBURG

Department of Chemistry and Molecular Biology
Gothenburg 2021

Water Condensation and Freezing in the Atmosphere:
Exploring Deliquescence and Ice Nucleation.

Cover illustration: Schematic illustration of water vapor - aerosol interactions, Dimitri Castarède and Hanna Danielsson.

ISBN: 978-91-8009-580-8 (PRINT)
ISBN: 978-91-8009-581-5 (PDF)

Department of Chemistry and Molecular Biology
University of Gothenburg
SE-412 96 Sweden

Printed by Stema AB
Borås, Sweden 2021

ABSTRACT

Atmospheric aerosols play key roles in numerous atmospheric processes. They affect human health, are substrates and components for atmospheric chemistry, and via their contribution to clouds affect the water cycle and the energy balance of the planet. The role of aerosols in these processes involves large uncertainty and this partly comes from an incomplete understanding of the aerosol phase state in the atmosphere. In fact, as aerosols travel through the atmosphere they may be exposed to temperature and humidity conditions that alter their properties. Although some of the mechanisms involved such as the deliquescence of soluble particles and the nucleation of cloud droplets are reasonably well understood. Others, like hygroscopic growth below deliquescence and heterogeneous ice nucleation remain poorly understood. This thesis aims to fill some of these knowledge gaps. For clarity, the report is thematically separated between *Pre-Deliquescence* that has contributed to three published papers (**Papers I**, **II** and **III**) and *Ice Nucleation*. *Ice Nucleation* involves significant instrumentation development and has contributed to one measurement report (**Paper IV**) and one technical paper presenting the developed instrument (**Paper V**).

I. Pre-Deliquescence
Soluble particles are characterized by their ability to dissolve into liquid water. They take part in unique processes such as their complete solvation into brine droplets below water saturation (*deliquescence*); and their surface solvation into thin liquid films below deliquescence (*pre-deliquescence*). The transition from solid soluble particles to liquid droplets is typically captured by Köhler theory which describes a modified equilibrium vapor pressure due to (i) mixing entropy (Raoult's law) and (ii) droplet geometry (Kelvin effect). However, this description omits the existence of a pre-deliquesced state. Therefore we develop a more complete model that accounts for interfacial forces giving rise to pre-deliquescence, in a manner akin to surface melting [26, 44]. The validity of the model is tested against previous hygroscopicity measurements of sodium chloride particles [7, 43] and results show that the model is able to reproduce observations using a set of physically realistic parameters. In **Papers II** and **III** the surface chemical composition of two common atmospheric salts, sodium acetate and ammonium sulfate, is observed at pre-deliquescence conditions using an ambient pressure X-ray photoelectron spectroscopy method. On the sodium acetate sample, reversible water uptake and salt dissociation is observed as humidity increases. Furthermore, a sodium depletion is observed at the sample surface after completing a deliquescence/efflorescence cycle. This is attributed to the formation of acetic acid and its enrichment at the liquid/gas interface. In the case of ammonium sulfate, species other than the salt ions are detected showing that chemistry takes place within the

pre-deliquesced film. S^0, HS^-, HONO, and $NH_{3(aq)}$ appear simultaneously to salt solvation and a chemical mechanism is suggested to explain the presence of these species.

II. Ice Nucleation and PINCii

The ice phase represents ≈ 65% of the total condensed water of clouds over the planet [115, 116] and is thus a key component in understanding the role of clouds on the radiative budget of the planet and on the hydrological cycle. In most tropospheric conditions (0°C ≥ T ≳ -37°C), ice crystals result from heterogeneous nucleation processes requiring the presence of specific particles. On average, only 1 in 10^6 atmospheric particles can act as a suitable surface for ice nucleation [29] and identifying these particles is key to understanding atmospheric ice nucleation and the development of cloud models. For this purpose, a large part of my PhD was invested in the development of a new portable ice nucleation chamber - PINCii. The details and evaluation of the PINCii instrument are presented in **Paper V** showing that PINCii is able to reproduce well defined activation processes such as homogeneous freezing, deliquescence and droplet formation with great accuracy. Results also show that PINCii can perform both ice nucleation and water droplet formation experiments with lower instrumental uncertainties than previous instruments of the same type. The HyICE-2018 field campaign based at the Smear II station in Hyytiälä (Finland) is presented in **Paper IV**. This campaign gathered various types of ice nucleation instruments in order to quantify the concentrations and identify the sources of ice nucleating particles in the boreal environment. Specific days were selected for ice nucleation instruments to run in parallel and at similar experimental conditions for inter-comparison purposes. **Paper IV** summarizes the aerosol properties and meteorological conditions during the campaign. It also presents the results of the inter-comparisons showing the amplitude of the deviations between the instruments present on site.

Keywords: Hygrscopicity, pre-deliquescence, adsorption, soluble particles, ice nucleation, PINCii.

SAMMANFATTNING

Atmosfäriska aerosoler spelar en nyckelroll i flera atmosfäriska processer. De påverkar människors hälsa, är substrat och komponenter för atmosfärisk kemi och via sitt bidrag till moln påverkar de vattnets kretslopp och jordens energibalans. Aerosolernas roll i dessa processer är förknippat med stora osäkerheter och beror det beror till viss del på okunskap kring aerosolers fastillstånd i atmosfären. När aerosoler färdas i atmosfären kan de exponeras för både temperatur och luftfuktighets förhållanden som kan förändra deras egenskaper. Även om en del mekanismer så som deliquescence av lösliga partiklar och kärnbildning av molndroppar är tämligen väl studerade, förblir andra processer som pre-deliquescence och heterogen kärnbildning av is dåligt förstådda. Denna avhandling syftar till att fylla några av dessa kunskapsluckor. För tydlighetens skull är avhandlingen tematiskt separerad mellan *Pre-Deliquescence* som har bidragit till tre publicerade artiklar (**Artikel I**, **II** och **III**) och *Ice Nucleation*. *Ice Nucleation* innefattar betydande instrument utveckling och har bidragit till en mät rapport (**Artikel IV**) och en teknisk artikel som presenterar det utvecklande instrumentet (**Artikel V**).

I. Pre-deliquescence

Lösliga partiklar karaktäriseras av deras förmåga att upplösas i flytande vatten. De deltar i unika processer så som deras fullständiga upplösning till saltvatten droppar under vatten mättnadsgrad (*deliquescence*); och deras ytas upplösning till tunn flytande film under deliquescence (*pre-deliquescence*). Övergången från fasta lösliga partiklar till flytande droppar är vanligtvis skildrad av Köhlers teori som beskriver ett modifierat jämvikts ångtryck på grund av (i) blandnings entropi (Raoult's lag) och (ii) dropp geometri (Kelvin effekt). Emellertid utelämnar denna beskrivning förekomsten av ett pre-deliquescence stadie. Därmed utvecklar vi en mer komplett modell som tar hänsyn till krafter vid ytgränssnitt som ger upphov till pre-deliquescence, på ett sätt som liknar ytsmältning [26, 44]. Modellens validitet prövas mot tidigare hygroskopicitet mätningar av natriumklorid partiklar [7, 43] och resultatet visar att modellen kan reproducera observationerna genom att använda fysiskt realistiska parametrar. I **Artikel II** och **III** observeras den kemiska komposition hos ytan av två vanliga atmosfäriska salter, natriumacetat och ammoniumsulfat under pre-deliquescence förhållanden, genom att använda ambient pressure X-ray photoelectron spectroscopy metoden. För båda salterna observeras reversibelt vatten upptag och salt upplösning medan luftfuktighet ökar. Vidare upptäcks andra arter än saltjoner som visar att kemiska reaktioner pågår innanför filmen av pre-deliquescence. På natriumacetat provet observeras en berikad yta av ättiksyra på grund utav rekombinationen av acetatjoner och vätejoner. I fallet med ammoniumsulfat uppkommer mellanarter så som S^0, HS^-, HONO,

and $NH_{3(aq)}$ samtidigt som salt upplösning således föreslås en kemisk mekanism förklara arternas närvaro.

II. Ice Nucleation and PINCii

Is fasen representerar ≈ 65% av allt kondenserat vatten hos moln i atmosfären [115, 116] och är således en viktig del i förståelsen av molnens inflytande på jordens strålningsbudget och i den hydrologiska cykeln. I de flesta troposfäriska förhållanden (0°C ≥ T ≳ -37°C) skapas iskristaller genom heterogena kärnbildningsprocesser som kräver närvaro av specifika partiklar. I genomsnitt kan endast 1 av 10^6 partiklar i atmosfären agera som en lämplig yta för kärnbildning av is [29] och identifierandet av dessa partiklar är nyckeln till förståelsen för atmosfärisk kärnbildning av is och utveckling av modellering av moln. För detta syfte har en stor del av mitt forsknings arbete varit investerat i utvecklandet av en ny portabel kammare för kärnbildning av is - PINCii. Detaljerna och utvärderingen av PINCii är presenterade i **Artikel V** som visar att PINCii kan reproducera väl definierade kärnbildningsprocesser som homogen frysning, deliquescence och skapandet av vattendroppar med god precision. Resultaten visar att PINCii kan utföra experiment för både kärnbildning av is och för skapande av vattendroppar med mindre osäkerheter än tidigare instrument av samma typ. Fältkampanjen HyICE-2018 på Smear II stationen i Hyytiälä (Finland) är presenterad i **Artikel IV**. Kampanjen samlade olika typer av instrument för kärnbildning av is för att kvantifiera koncentrationen och identifiera kärnbildnings partiklarnas källa i den boreala miljön. Specifika dagar valdes ut för en samtida körning av kärnbildnings instrumenten under liknande experimentella förhållanden i jämförelse syfte. **Artikel IV** sammanfattar aerosol egenskaperna och de metrologiska förhållandena under kampanjen. Den presenterar även resultatet av jämförelsen mellan de olika instrumenten och visar amplituden för avvikelserna mellan instrumenten på plats. Nyckelord: Hygroskopicitet (vattenupptagningsförmåga), pre-deliquescence, adsorption, lösliga partiklar, is kärnbildning, PINCii.

Nyckelord: Hygroskopicitet (vattenupptagningsförmåga), pre-deliquescence, adsorption, lösliga partiklar, is kärnbildning, PINCii.

List of Publications

This thesis is based upon the following five papers. These papers are appended in **Part II** and referred to in **Part I** by their roman numerals (I-V).

I. **A thermodynamic description for the hygroscopic growth of atmospheric aerosol particles.**
Castarède D & Thomson ES. Atmospheric Chemistry and Physics. 2018 Oct 17; 18(20):14939-48. doi: 10.5194/acp-18-14939-2018 | Note! Supplementary material included in Part II.

II. **Reversibly physisorbed and chemisorbed water on carboxylic salt surfaces under atmospheric conditions.**
Kong X, **Castarède D**, Boucly A, Artiglia L, Ammann M, Bartels-Rausch T, Thomson ES & Pettersson JBC. The Journal of Physical Chemistry C. 2020 Feb 5; 124(9):5263-9. doi: 10.1021/acs.jpcc.0c00319 | Note! Supplementary material available online.

III. **A surface-promoted redox reaction occurs spontaneously on solvating inorganic aerosol surfaces.**
Kong X, **Castarède D**, Thomson ES, Boucly A, Artiglia L, Ammann M, Gladich I & Pettersson JBC. Science. 2021 Nov; 374(6568):747–752. doi: 10.1126/science.abc5311 | Note! Supplementary material available online.

IV. **Measurement report: Introduction to the HyICE-2018 campaign for measurements of ice nucleating particles in the Hyytiälä boreal forest.**
Brasseur Z, **Castarède D**, Thomson ES, Adams MP, Drossaart van Dusseldorp S, Heikkilä P, Korhonen K, Lampilahti J, Paramonov M, Schneider J, Vogel F, Wu Y, Abbat JPD, Atanasova NS, Bamford DH, Bertozzi B, Boyer M, Brus D, Daily MI, Fösig R, Gute E, Harrison AD, Hietala P, Höhler K, Kanji ZA, Keskinen J, Lacher L, Lampimäki M, Levula J, Manninen A, Nadolny J, Peltola M, Porter GCE, Poutanen P, Proske U, Schorr T, Umo NS, Stenszky J, Virtanen A, Moisseev D, Kulmala M, Murray BJ, Petäjä T, Möhler O & Duplissy J. Atmospheric Chemistry and Physics Discussions. 2021 Oct; 8:1-46. doi: 10.5194/acp-2021-744

V. **Development of the Portable Ice Nucleation Chamber PINCii.**
Castarède D, Brasseur Z, Wu Y, Kanji ZA, Bilde M, Stratmann F, Swietlicki R,

Svenningsson B, Sierau B, Stetzer O, Nguyen QT, Pettersson JBC, Duplissy J & Thomson ES. Manuscript for submission to Atmospheric Measurement Techniques.

Statement of Contribution

I. Dimitri Castarède (DC) fully developed the thermodynamic model presented in Paper I under the supervision of Erik S. Thomson (EST). DC analyzed the data, did the theoretical calculations and comparisons with data and constructed all figures. The paper was written jointly.

II. DC participated in the data collection at the Swiss Light Source of the Paul Scherrer Institute. DC contributed to the discussions to explain the experimental observations and to the writing and revision of the manuscript.

III. DC participated in the data collection at the Swiss Light Source of the Paul Scherrer Institute. DC contributed to the discussions to explain the experimental observations and to the writing and revision of the manuscript.

IV. DC was on site for three months of the HyICE-2018 field campaign presented in Paper IV and during that time contributed to data collection. DC discussed and helped execute all the data analysis and constructed all figures except figures 4-6, 8-9 and 14. DC participated in the writing and revisions of the paper.

V. EST conducted the development of the first prototype of the instrument presented in Paper V. DC continued the project and built the following iterations of the instrument with the help of Zoé Brasseur and Yusheng Wu. DC designed engineering improvements, drew all 3D blue prints, expanded the software, mounted the chambers and connected all external components. DC performed all experiments for Paper V. He analyzed all data, constructed all the figures and wrote the manuscript under the supervision of EST.

Other Related Publications

I. **Interactions between the atmosphere, cryosphere, and ecosystems at northern high latitudes.**
Boy M, Thomson ES, Acosta Navarro JC, Arnalds O, Batchvarova E, Bäck J, Berninger F, Bilde M, Brasseur Z, Dagsson-Waldhauserova P, **Castarède D**, Daliran M, de Leeuw M, Dragosics M, Duplissy EM, Duplissy J, Ekman AML, Fang K, Gallet JC, Glasius M, Gryning SE, Grythe H, Hansson HC, Hansson M, Isaksson E, Iversen T, Jonsdottir I, Kasurinen V, Kirkevåg A, Korhola A, Krejci R, Kristrjansson JE, Lappalainen HK, Lauri A, Leppäranta M, Lihavainen H, Makkonen R, Massling A, Meinander O, Nilsson D, Olafsson H, Pettersson JBC, Prisle NL, Riipinen I, Roldin P, Ruppel M, Salter M, Sand M, Seland Ø, Seppä H, Skov H, Soares J, Stohl A, Ström J, Svensson J, Swietlicki E, Tabakova K, Thorsteinsson T, Virkkula A, Weyhenmeyer GA, Wu Y, Zieger P & Kulmala M. Atmospheric Chemistry and Physics. 2019 Feb 14; 19(3):2015-61. doi: 10.5194/acp-19-2015-2019.
Contribution: Data collected from HyICE-2018 campaign as presented in detail in publications IV and V was first published here. DC constructed Figures 2 and 7 for this paper.

II. **The seasonal cycle of ice-nucleating particles linked to the abundance of biogenic aerosol in boreal forests.** Schneider J, Höhler K, Heikkilä P, Keskinen J, Bertozzi B, Bogert P, Schorr T, Umo NS, Vogel F, Brasseur Z, Wu Y, Hakala S, Duplissy J, Moisseev D, Kulmala M, Adams MP, Murray BJ, Korhonen K, Hao L, Thomson ES, **Castarède D**, Leisner T, Petäjä T & Möhler O. Atmospheric Chemistry and Physics. 2021 Mar 16; 21(5):3899-918. doi:v10.5194/acp-21-3899-2021.
Contribution: DC was one of the primary participants in the HyICE-2018 campaign. He contributed to the writing and revisions of this manuscript.

Contents

Part I

THESIS

1

Background and Motivation

"Man stands face to face with the irrational. He feels within him his longing for happiness and for reason. The absurd is born of this confrontation between the human need and the unreasonable silence of the world."

Albert Camus.

Contents

1.1 The Atmosphere

The atmosphere is an envelope of gas covering the surface of the Earth. Its lowest layer the troposphere extends from the ground to $\approx 10-13$ km in altitude and it is within this layer that most interactions with the ground occur and where most clouds are formed. The composition of Earth's atmosphere constantly evolves. In early Earth history, it was similar to what volcanoes emit: carbon dioxide, water vapor and nitrogen. With time, the planet cooled and water vapor condensed to form oceans that then dissolved most of the carbon dioxide. Today's atmosphere still contains the originally present inert nitrogen (78%) but also provides us with oxygen (21%), water (up to 3%), carbon dioxide (0.04%) and other trace gases. Solid particles also exist in this gas mixture. They can be emitted from natural sources such as the ocean surface (salts), deserts (dust) or forests (biological particles) and also from anthropogenic activities (e.g., soot). Fig. 1.1 illustrates a snapshot of the distribution of those particles over the globe.

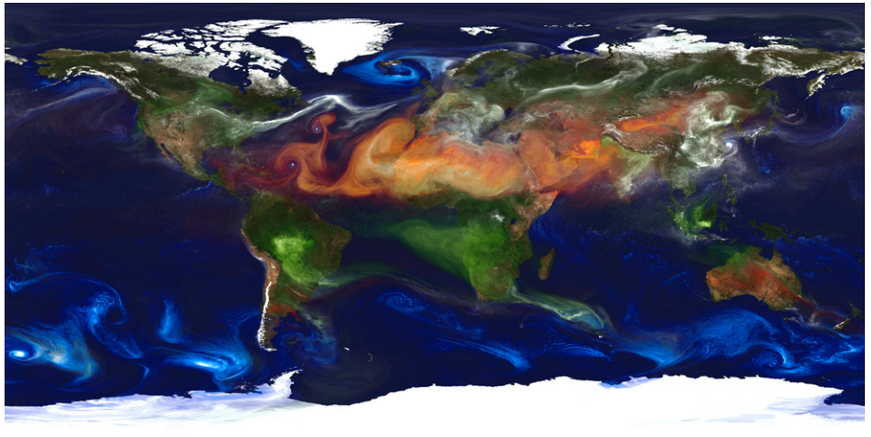

Figure 1.1: Simulation of global aerosols. Mineral dust in red, sea salt in blue, biomass burning in green, sulfate particles from natural and anthropogenic emissions in white. Image credit: William Putman, NASA/Goddard.

This mixture of gas and particles is not stationary, temperature gradients between the poles and the equator set in motion large scale circulations that constantly tend to homogeneize

atmospheric pressure and temperature. As winds carry water vapour and particles, clouds may appear in the process in various shapes and compositions.

1.2 Clouds and Hydrometeors

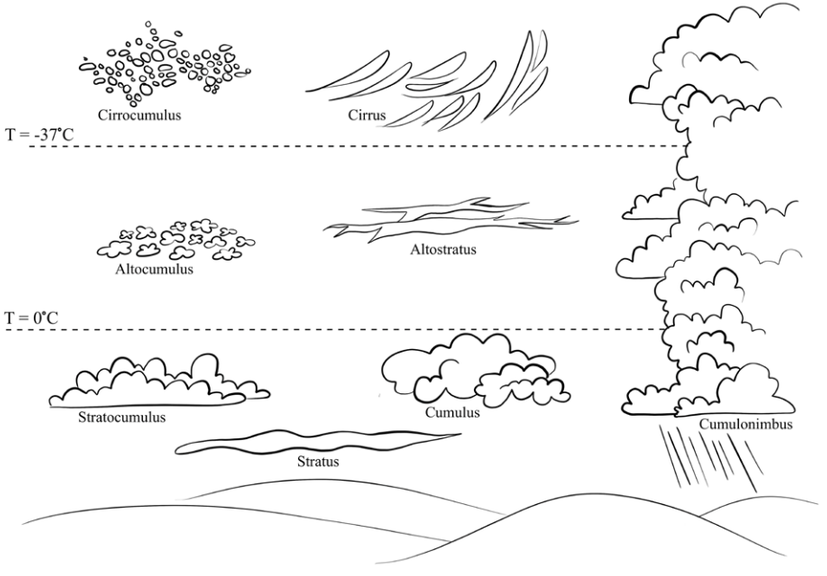

Figure 1.2: Schematic representation of different cloud types and the critical temperature changes (dashed lines) delimiting low level ($T > 0°C$) from mid level ($0°C \geq T \gtrsim -37°C$) and high level clouds ($T \lesssim -37°C$). Low level clouds are uniquely formed of water droplets, mid level clouds or mixed-phase clouds may be composed of both liquid water and ice and high level are clouds uniquely composed of ice.

The question of what clouds are was an early question in philosophers minds. In his work '*Meteoroligica*' published in 340 BC, Aristotle already had an intuition for crucial concepts such as water vapor and evaporation:

"Some of the vapour that is formed by day does not rise high because the ratio of the fire

that is raising it to the water that is being raised is small."

It was during the 1600's that the first meteorological instrumentation was invented and the first scientific studies aiming to understand the formation and properties of clouds were undertaken. This led to the discovery of crucial scientific concepts such as atmospheric pressure by Pascal in 1648, the development of thermodynamic models like the kinetic theory of gases by Bernouilli in 1738 and the ideal gas law by Clapeyron in 1834. The first cloud classification [51] published by Luke Howard in 1803 was also published during this time. An illustration of different clouds types described in this classification is presented in Fig. 1.2. Although this classification was mostly based on superficial characteristics of clouds such as height, shape (and electrical properties), it was later found that these characteristics are also good proxies for more fundamental underlying properties such as composition, life-time and even radiative effects. It is now clear that clouds are masses of ice crystals or water droplets suspended in the air (hydrometeors). The phase of these hydrometeors depends on the Temperature (T) during their formation and evolution. In Fig. 1.2, three cloud categories are distinguished, (i) warm clouds formed at T > 0°C are composed of water droplets, (ii) mixed-phase clouds formed at 0°C ≥ T ≳ -37°C are a mixture of both super-cooled water droplets and ice crystals, and (iii) cold clouds or high clouds formed at T ≲ -37°C are only composed of ice crystals. Temperature is not the only variable determining the phase state and stability of the hydrometeors, the Relative Humidity (RH) is also a determining factor.

With RH_{liq} the RH with respect to liquid water and RH_{ice} with respect to ice, the RH represents the vapor pressure p normalized by the equilibrium vapor pressure of the given phase p_{liq} or p_{ice}. With equilibrium vapor pressure representing the theoretical vapor pressure required to keep a given system at equilibrium so that the condensation rate of water vapor on its surface balances its evaporation at a given temperature. RH can thus be calculated as follows: $RH_{liq} = \frac{p}{p_{liq}} \times 100$. At RH = 100%, the respective phases are found at equilibrium whereby the rate of evaporation of water molecules from a surface is equal to the rate of condensation of water vapor on the surface; at RH < 100%, the condensate is under-saturated meaning that it will evaporate faster than the available vapor can condense on its surface which will result in a net evaporation. Alternatively a super-saturated system (RH > 100%) will have a net condensation and growth.

Depending on the balance of forces keeping them in suspension and the RH/T conditions, hydrometeors can range from hundreds of nanometers to millimeters in size, as illustrated in Fig. 1.3. Once their growth allows them to overcome buyouancy, they may sediment as precipitation. Clouds are thus an important part of the water cycle recirculating atmospheric

water back to the ground.

Clouds also have important and complex climate implications. They cover around two thirds of the Earth's surface at any given moment [30, 131] and can interact with both the incoming solar radiation and the outgoing long-wave radiation from the Earth surface. Therefore, depending on their shape, composition, height, and life-time, their response to the radiative forcing exerted by the sun may vary.

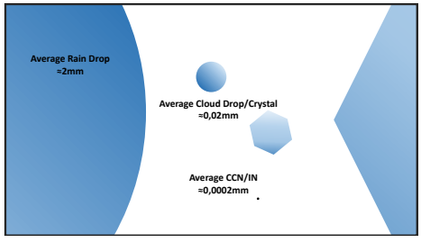

Figure 1.3: Schematic representation of the aerosol composition of a cloud. This picture illustrates that large exchanges of water vapor are required to go from the nucleation of a cluster on a CCN/IN surface to a hydrometeor able to precipitate.

From the definition of clouds presented above, it is clear that cloud formation requires the condensation of water vapor to form either water droplets or ice crystals and that this condensation is driven by T and RH. However, water vapor rarely condenses on its own to create a stable new phase (*homogeneous nucleation*) in Earth's atmosphere, as this requires RH/T conditions that are not typically found. In order to understand these limitations and explain how the formation of hydrometeors is actually possible, an understanding of some key micrcophysical processes is required.

1.3 Microphysical Processes

From adsorption of a few water molecules on a particle surface, to the formation of a stable cluster and its growth to a hydrometeor size. Cloud hydrometeors result from a series of nano/micro-physical processes that bring large amounts of water molecules together as a result of changing environmental conditions.

1.3.1 Nucleation

An atmospheric hydrometeor is created when random collisions of water molecules result in the formation of a stable liquid/solid condensate. This phase change, called nucleation, is possible if the created new phase is more energetically favorable than the parent phase it emerges from. This can be quantified by calculating the chemical potential of the respective phases. However, although the bulk of the new phase may be more energetically favorable than the bulk of its parent phase, it is not the case for its interface. The parent phase must therefore enter a meta-stable state (e.g., vapor super-saturation, liquid super-cooling) where the total cost of creating the new phase (bulk + interface) becomes more energetically favorable than the parent phase it emerges from. This process may happen as described (*homogeneous nucleation*) or with the help of a third body that may lower the energy cost of creating the interface (*heterogeneous nucleation*).

1.3.1.1 Homogeneous Nucleation

Homogeneous nucleation is the phase transition that occurrs when within a bulk parent-phase (e.g., vapor), an unstable daughter-cluster (e.g., liquid) of radius r grows beyond a critical radius r^* by random collisions and arrangements of water molecules to become more energetically favorable than the parent-phase from which it emerges. It can be mathematically described by considering the Gibbs free energy difference ΔG between the system including the formed daughter phase from the original parent phase system. The Gibbs free cost(positive) / gain(negative) to form the daughter phase is described in Eq. 1.1,

$$\Delta G = -\frac{4}{3}\pi r^3 \Delta\mu + 4\pi r^2 \gamma, \tag{1.1}$$

with $\Delta\mu$ the difference in chemical potential between the parent phase and the new phase and γ the surface free energy at the interface between the parent and the daughter phases.

The first term in Eq. 1.1 represents the energy gained from forming the daughter phase while the second term describes the free energy cost to create the interface. This is thus an activated process where the energy penalty of forming the daughter-phase surface needs to be overcome. This limitation explains why air masses need to be supersaturated in water vapor in order to nucleate hydrometeors and why water droplets need to be super-cooled in order to freeze. It also explains why droplets take a spherical shape that minimizes their surface/volume (energy penalty/gain) ratio. The evolution of the surface and volume terms with size r can be seen in Fig. 1.4 where the formation of a stable new cluster occurs at $r = r^*$ and $\Delta G = \Delta G^*$. Homogeneous nucleation from vapor to liquid/ice is typically not achieved in the troposphere because the temperature/pressure conditions required to overcome the energy barrier do not occur. In fact, relative humidity rarely exceeds 101% in common tropospheric clouds [66] and homogeneous nucleation from a pure water vapor phase would require $RH_{liq} \gtrsim 150\%$ [128, 132]. The atmospheric nucleation of water droplets and ice crystals thus typically occurs through heterogeneous nucleation processes only. On the other hand, homogeneous nucleation from water droplets to ice crystals does occur in the atmosphere. It can be responsible for the freezing of super-cooled droplets in high clouds as it becomes spontaneously possible at T $\lesssim$ -37°C [64, 86]. However, most tropospheric ice forms in warmer conditions from heterogeneous nucleation processes.

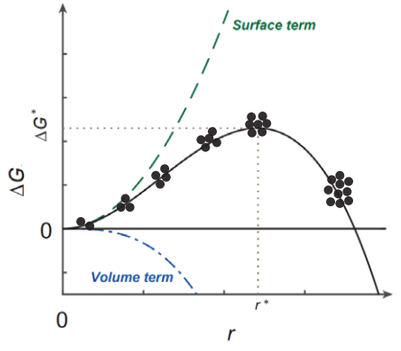

Figure 1.4: Schematic of the contributions from surface (green) and volume (blue) terms in Eq. 1.1 to the Gibbs free energy barrier. A cluster is formed from the stochastic coallisions of molecules and becomes stable if its size overcomes the nucleation barrier at $r = r^*$ and $\Delta G = \Delta G^*$. Figure adapted from Mahrt, 2019 [76].

1.3.1.2 Heterogeneous Nucleation

Solid particles may facilitate nucleation processes by acting as nuclei on which water molecules can agglomerate. This diminishes the surface area required to form the interface

and thus diminishes the free energy barrier to forming the condensate. Put simply, the energy cost of forming an interface is diminished if an existing surface can facilitate cluster formation. However, not all surfaces catalyze nucleation with the same efficiency and many surface parameters influence this process. For example, the interfacial free energy between the nucleus and the cluster, the porosity of the surface, the solubility of the surface, and molecular scale interactions with the surface. A solid particle acting as a nuclei for the formation of a water droplet is termed a Cloud Condensation Nuclei (CCN) while the nucleus of an ice crystal is called an Ice Nucleating Particle (INP) [122]. In the atmosphere, most clouds result from heterogeneous processes that involve the presence of CCNs or INPs and while the properties of good CCNs are well defined [70], the characteristics of good INPs remain uncertain [56].

1.3.2 Adsorption

Nucleation involves a significant number of water molecules because the formed bulk needs to be large enough to overcome the penalty of creating its interface. However, clusters and films of water molecules have been observed to be stable on surfaces well below the r^* and T/RH conditions required for nucleation. This molecular scale formation of water clusters is referred to as adsorption. Adsorption cannot be represented by standard bulk thermodynamics because at the molecular scale, consideration of inter-molecular forces needs to be implemented. Adsorption phenomena is thus traditionally explained by two types of inter-molecular interactions: dispersion and Debye forces. Dispersion forces are weak long range forces originating from the chaotic movement of the electronic cloud of a molecule creating a temporary dipole able to induce and attract the electronic cloud of another compound [37, 38]. Debye forces on the other hand, are forces representing the induction created from a permanent dipole (e.g., water molecule) towards the electronic cloud of a neighbor molecule to create an attractive force. Debye forces are observed between any polar molecule and non-polar molecule and are stronger than the dispersion forces.

1.3.3 Other processes

Adsorption and nucleation are very important processes because they are the starting point for water condensation in the atmosphere. However, in order for a newly formed cluster to grow to hydrometeor sizes, large amounts of water molecules need to be brought together as illustrated in Fig. 1.3. Therefore, other processes such as condensational and collisional growth are required to complete the cloud formation process. Although these are important processes to consider especially when thinking about how micro-physical processes scale up to observable macro-physical phenomena, they are beyond the scope of this thesis work.

1.4 Motivation and Aim

Atmospheric aerosols play important roles in many aspects of the physics and chemistry of the atmosphere [8]. They affect human health via inhalation causing more than four millions premature deaths per year [108]. They can catalyze atmospheric chemistry [4, 63] by providing a medium for species to react and contribute to many important chemical mechanisms such as halogen chemistry [40], ozone depletion [13], secondary organic aerosol formation [41], etc. Through the formation of clouds and precipitation, aerosols play an important part of the hydrological cycle recirculating atmospheric water back to the ground. They also affect the energy balance of the planet through direct and indirect mechanisms [1, 32, 73]. In fact, aerosols can absorb and scatter short-wave solar and long-wave terrestrial radiation and thus directly influence the energy balance of the planet. Furthermore, they can induce various indirect feedbacks such as altering the albedo of ice and snow surfaces in Arctic regions [1, 9] or influencing clouds properties [32]. However, aerosols are subject to micro-physical processes (cf. § 1.3.) that may alter their properties. Although some of the mechanisms involved, such as water adsorption on non-soluble particles [42, 49, 67] or the homogeneous freezing of super-cooled droplets [64], are well resolved. Others, such as water adsorption on soluble particles and heterogeneous ice nucleation, remain poorly understood. The incomplete understanding of such mechanisms typically results in significant uncertainties within the effects of aerosols [4, 8, 94, 95]. This thesis aims to fill some of these knowledge gaps and has focused on two separate themes: water adsorption on soluble particles and ice nucleation. Therefore, this report is divided into two chapters titled: *Pre-Deliquescence* and *Ice Nucleation and PINCii*.

Pre-Deliquescence aims to improve understanding on salt-water interactions in the atmosphere. Sea salt particles are the second most abundant aerosol particle species [71, 101] and are known for their hygroscopic behavior and their ability to adsorb water at very low humidity, which has been observed through numerous experiments [7, 18, 43, 119]. As the extent of this water uptake cannot be explained by common adsorption theories developed for non-soluble particles, theoretical explanations, parameterizations and the possible atmospheric implications of such systems are unclear. **Paper I** aimed to build a thermodynamic model to explain and capture the hygroscopic behavior of pure salts in atmospherically relevant conditions. **Papers II** and **III** use experimental observations to examine the potential implications of such systems on atmospheric chemistry. Using the APXPS method (cf. § 2.3.1), chemical analyses were performed to investigate chemical

reactions taking place on the surface of atmospherically relevant salts as water adsorbs onto their surfaces.

The second part *Ice Nucleation and PINCii*, presents the development of a new ice nucleation instrument that contributes to the data collection and the development of knowledge of heterogeneous ice nucleation. Ice crystals represent $\approx 65\%$ of the total hydrometeor population of clouds over the planet [115] and a large fraction results from heterogeneous nucleation processes. However, what makes a particle a good INP is unclear and being able to identify and quantify INPs in various environments may greatly improve the efficiency of cloud simulations. To this purpose, **Paper V** presents the development, construction, and evaluation of a new ice nucleation chamber that will improve on some common limitations of previous instruments and in the future be able to contribute to the collection of INP measurements. **Paper IV** introduces a field campaign that took place in Hyytiälä (Finland) in 2018. This campaign aimed to bring together different types of ice nucleation instruments in order to inter-compare them in a natural environment, quantify inter-instrumental deviations and provide a meteorological summary that will be used as the basis of comparison for many campaign activities.

2

Pre-Deliquescence

"If we believe in nothing, if nothing has any meaning and if we can affirm no values whatsoever, then everything is possible and nothing has any importance."

Albert Camus.

Contents

2.1 Background

The most efficient and abundant CCN in the atmosphere are large soluble particles [70]. Soluble particles can dissolve into condensing water and decrease the vapor pressure required for nucleation. Put simply, the presence of dissolved material at the liquid/gas interface decreases the equilibrium vapor pressure of the system by limiting the evaporation of water molecules [98]. Soluble particles such as salts thus activate below pure water saturation ($RH_{liq} < 100\%$), at a specific relative humidity called the Deliquescence Relative Humidity (DRH), forming a droplet saturated in dissolved material [78]. This process called deliquescence is a mechanism that leads to the formation of atmospheric water droplets below $RH_{liq} = 100\%$, and explains why soluble particles are considered the best CCN. The deliquescence transition is traditionally modelled by Köhler theory which predicts DRH by calculating the equilibrium vapor pressure over the formed saturated brine droplet. Köhler theory also captures the size evolution of this brine droplet with changing humidity assuming equilibrium conditions [61]. To accomplish this, Köhler theory is built upon two parameters which describe how droplet stability is affected by the interfacial curvature and the presence of dissolved material [33, 74]. Thus the equilibrium vapor pressure p_r over a brine droplet is described by the cumulative influences of the curvature and the solute effects in analogy to their departure from the equilibrium vapor pressure $p_{b\infty}$ over a flat pure water surface,

$$\frac{p_r}{p_{b\infty}} = \frac{p_{sol}}{p_{b\infty}} \cdot \frac{p_r}{p_{sol}}, \tag{2.1}$$

where p_{sol} represents the equilibrium vapor pressure over a flat solution. The solute effect [98] presented as the first term in Eq. 2.1 can be given by theoretical models [22, 134] or empirical parameterizations that best match the system of interest [119]. Likewise the curvature term presented as the second term in Eq. 2.1 is given by the Kelvin equation.

Although deliquescence is viewed as an abrupt and spontaneous process, measurements show the presence of liquid water on salt particles well below the DRH [7, 12, 18, 31, 43, 75, 91, 123, 129]. This water uptake below DRH has been observed to be (i) reversible [12, 62, 129]; (ii) to trigger the solvation of a fraction of the salt [17, 129, 130]; (iii) and to exceed molecular scale adsorption (cf. §1.3.2) [12, 129]. It is thus differentiated from standard adsorption phenomena and will be referred to as *pre-deliquescence*. Adsorption processes that take place on non-soluble particles are well modelled using adsorption isotherms [42, 49]. Such systems are better defined and theories such as the one described

in Laaksonen et al., 2015 [67] capture the complete transition from dry materials gradually adsorbing water vapor to the supersaturations required for bulk water. However, fewer theories exist to capture the complete evolution of soluble particles [80, 81, 113] and thus hint that Köhler theory can be refined to model this liquid phase, which represents an unconsidered atmospheric aqueous reservoir. This has implications for the representation of soluble particles within climate models and has the potential to change our understanding of radiative effects as well as the surface chemistry of soluble particles in the atmosphere.

2.2 Pre-Deliquescence Theory

Paper I suggests a theoretical refinement of Köhler theory by considering the stability of a salt particle that is gradually engulfed and dissolved by a brine layer (Fig. 2.1). The model includes the traditional bulk phase parameters influencing the equilibrium of the system (solute and curvature effects) but invokes an interfacial term that accounts for the intermolecular forces acting within the system. This is accomplished in a manner akin to the pre-melting of ice [26, 44] where two different kinds of intermolecular forces are considered. First, electrostatic interactions that arise from the presence of a surface charge at the salt/solution interface [60, 72]. Second, dispersion forces originating from interactions between instantaneous dipoles and induced dipoles [37, 38, 44].

In order to re-express Köhler theory, we thus define the equilibrium vapor pressure p_ζ over a spherical charged salt coated by a saturated brine layer (Fig. 2.1), and thus in analogy to Eq. 2.1,

$$\frac{p_\zeta}{p_{b\infty}} = \frac{RH_{liq,\zeta}}{100} = \frac{p_{sol}}{p_{b\infty}} \cdot \frac{p_r}{p_{sol}} \cdot \frac{p_\zeta}{p_r}. \tag{2.2}$$

The added term $\frac{p_\zeta}{p_r}$ accounts for the effect of intermolecular forces on the system equilibrium. The complete derivation of the term can be found in **Paper I** and its supplementary material [14]. Eq. 2.2 can thus represent the equilibrium relative humidity $RH_{liq,\zeta}$ (with respect to liquid water) over a salt particle gradually dissolving at RH < DRH, deliquescing at DRH and reduces to the standard Köhler equation at RH > DRH to capture the complete transition from dry particle to brine droplet, as illustrated in Fig. 2.2. With growth factor the ratio of the system radius to its dry radius, Fig. 2.2 represents the water uptake on a 5 nm dry NaCl particle as a function of RH. The solid lines represent the system equilibrium captured by Eq. 2.2 with the individual terms of Eq. 2.2 represented as dashed lines.

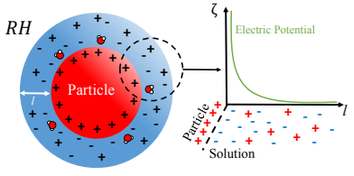

Figure 2.1: Schematic of the system considered herein – an idealized solvating atmospheric particle. The use of an idealized spherical geometry is justified by previous findings that NaCl crystal corner and step sites dissolve preferentially to surface sites, in a manner that quickly roughens and rounds faceted crystals [17, 129, 130]. Reproduced from **Paper I**.

This theory was used to model hygroscopicity measurements of NaCl particles from Hämeri et al., and Biskos et al., [7, 43] at various particle sizes and **Paper I** shows that the model well represents the experimental observations. However, as the properties of pre-deliquesced systems are not well defined in the literature, layer concentration, surface charge and the strength of dispersion forces (Hamaker constant) have been kept as free parameters and minimized in a non-linear least-squares comparison with the experimental results. Results showed that the surface charge(s) and Hamaker constant(s) that emerge are reasonable compared to previously reported values [44, 60]. The minimized layer concentration(s) are also in agreement with literature values of saturated NaCl solutions [47]. However, when the model is applied to particles with a dry radius $R_s \lesssim 20$ nm, the minimized concentrations showed an exponential increase with decreasing particle size as shown in Fig. 2.3. These unrealistic values at $R_s \lesssim 20$ nm may be the result of the model compensating for other physical effects not made explicit in this study. For example surface free energy depletion [5, 102]. Such effects could lower the free energy of the liquid phase at very small sizes.

Paper I also discusses the potential implications of this model and the importance of such systems in the atmosphere. This model might for example have implications in the stability of mixed phase clouds and partially explain their persistence. Mixed-phase clouds are thermodynamically unstable due to the difference in equilibrium vapor pressure between the ice and the liquid phases. In fact, according to the Wegener–Bergeron–Findeisen (WBF) process [6, 36, 126] the equilibrium vapor pressure difference between the phases should lead to a diffusion of water vapor and a growth of the ice phase at the expense of the liquid phase. As Morrison et al., 2012 [84] stated:

"This microphysical instability (WBF Process) can transform mixed-phase clouds to ice-

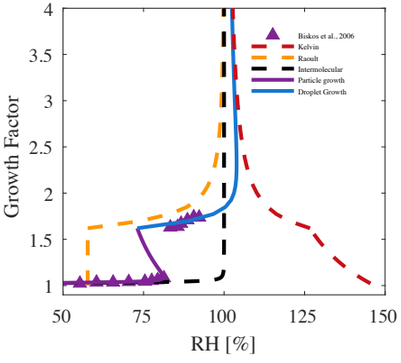

Figure 2.2: The evolution of the individual terms in Eq. 2.2 are shown for a solvating 5 nm NaCl particle. For such small particles the Kelvin term dominates, yielding an activation barrier, as illustrated by the inflection in the layer growth (magenta) curve. One also observes that the Raoult term (yellow curve) changes only after the solid particle dissolves (DRH) and that the intermolecular interactions are very short range (black curve). Reproduced from **Paper I**.

only clouds within a few hours or less [46, 54, 92, 97]. Consequently, the persistence of these clouds for periods of days to weeks [109, 124, 135] is unexpected."

Numerous explanations for mixed phase persistence have been proposed [84], like droplet growth via radiative cooling of the cloud top [24, 107, 111], and the relative occurence of the WBF-conditions ($\frac{p_{ice}}{p_{bo\infty}} \times 100 < RH_{liq} < 100\%$) within mixed phase clouds [65]. However, the relative contributions of these explanations have not yet been quantified and the issue still remains under debate.

As described in **Paper I**, pre-deliquesced thin films are meta-stable in a wide range of RH conditions and the equilibrium vapor pressure over a pre-deliquesced particle may thus be less than the equilibrium vapor pressure of ice. By extending the principles of the WBF process to a more complex system including pre-deliquesced particles, vapor diffusion from ice crystals to pre-deliquesced particles may recycle water vapor towards the liquid phase and potentially extend the lifetime of the mixed-phase as illustrated in Fig. 2.4. Theoretically this re-circulation towards the liquid phase is valid in scenarios where at DRH $> RH_{liq} > \frac{p_{ice}}{p_{bo\infty}} \times 100$, a continuous growth of the ice phase in this super-saturated regime may be attenuated by a diffusion of water molecules towards pre-deliquesced particles that are meta-stable below DRH. Alternatively at $\frac{p_\zeta}{p_{bo\infty}} \times 100 < RH_{liq} < \frac{p_{ice}}{p_{bo\infty}} \times 100$, a growth of pre-deliquesced particles can occur at the expense of the ice phase that is evaporating in

the sub-saturated environment, thus recirculating water vapor from the ice to the liquid phase.

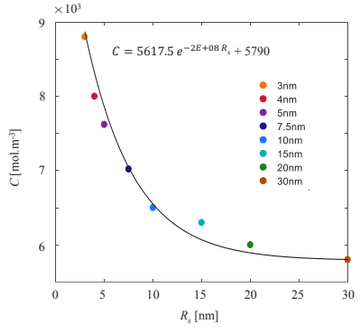

Figure 2.3: Summary of the brine layer concentration C values derived to match experimental hygroscopicity data of various-sized particles [7, 43]. A fit to these values is also added to show the exponential dependence between particle size and the concentration values needed to match hygroscopicity data. For reference, the saturated concentration of a bulk NaCl solution at room temperature is $\approx 5.4\times10^3$ mol $\cdot$ m^{-3} [47].

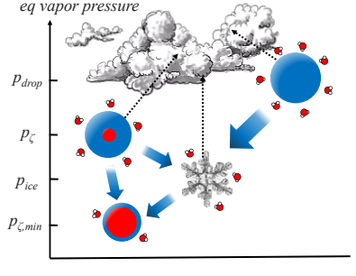

Figure 2.4: Schematic of the equilibrium vapor pressures over droplets, pre-deliquesced particles, and ice particles, where gradients lead to Wegener–Bergeron–Findeisen processing. The range of equilibrium vapor pressures above pre-deliquesced thin films straddle the equilibrium vapor pressure over ice p_{ice}, resulting in a more stable coexistence between ice and pre-deliquesced particles, relative to liquid droplets. Reproduced from **Paper I**.

2.3 APXPS

Complementing the work done in **Paper I**, **Papers II** and **III** present studies resulting from Ambient Pressure X-ray Photoelectron Spectroscopy (APXPS) measurements. These studies were conducted to investigate the surface behaviour, dissolution and potential chemistry of common atmospheric salts (sodium acetate and ammonium sulfate) over a range of RH covering pre-deliquescence and up to the DRH.

2.3.1 Methods

X-ray Photoelectron Spectroscopy (XPS) uses X-rays to irradiate a surface and probe its chemical composition. Electrons from the atoms present on the surface exposed to high energy photons are ejected. A fraction of the ejected electrons is detected and the electrons kinetic energy is measured. From a measured electron kinetic energy, its binding energy ($E_{binding}$) to the atom to whom it belonged can be calculated as: $E_{binding} = E_{Xray} - (E_{kinetic} + \Phi)$ with E_{Xray} the energy of the X-ray photons used to probe the surface, $E_{kinetic}$ the kinetic energy of the ejected electron and Φ a work function that is instrument-dependant and describes the difference between Fermi level and vacuum level. The energy binding an electron to its nucleus is unique and can be used as a signature to identify the elements present on the sample surface as well as oxidation states, and degrees of dissociation. However, these methods usually require high vacuum conditions as the emitted electrons have a very short mean free path and would otherwise be attenuated in the gas phase. The APXPS method [88] uses a cell to separate a pressurized inner chamber containing the desired sample surface and gas composition from a high vacuum outer chamber that allows X-ray transmission from the source to the inner chamber and electron transmission out. The cell is made of stainless steal and the X-ray window is made of silicon nitrite, a X-ray transparent material. This allows the transmission of photons while maintaining the pressure gradient across the cell up to 20 mbar [88]. The vapor pressure in the inner chamber chamber is controlled by filling from an external gas volume that has been set at equilibrium with a liquid water reservoir which is temperature controlled. The RH in the inner chamber can be changed during experiments by changing the temperature of the

gold-coated sample holder using a pelletier element. From the set vapor pressure in the chamber, one can calculate the temperature required to get the desired RH.

Both **Papers II** and **III** present APXPS experimental results performed at the "in situ spectroscopy" beamline of the Swiss Light Source (SLS) at the Paul Scherrer Institute (PSI) in Switzerland; using the synchrotron as a X-ray source. All the salt samples analyzed were subject to the same treatment prior to measurements. Samples are dissolved in water and drop-cast onto the sample holder. Once the sample holder is placed within the inner chamber, a complete deliquescence/efflorescence cycle is performed in order to homogenize the sample on the holder.

2.3.2 Results

In **Paper II**, the surface behaviour of a carboxylic salt (Sodium Acetate) is investigated at pre-deliquescence and deliquescence conditions. Sodium Acetate ($C_2H_3NaO_2$) was chosen for its atmospheric relevance in numerous chemical reactions [15] and its abundance as it is a product of sodium chloride and acetic acid. Acetic acid is widely emitted from anthropogenic activities [57, 118], natural sources [58] and is an important product of common volatile organic compounds. Using the APXPS method, several key observations were made.

First, water adsorption and salt solvation are both observed as RH is incrementally increased below DRH and if RH is decreased both these processes appeared reversible. These observations are consistent with previous experimental observations [12, 17, 62, 129, 130] and support the meta-stable nature of the pre-deliquescence system described in **Paper I** [14]. Furthermore, water adsorption on the salt surface is observed at very low humidity (RH $\gtrsim$ 3%). However, salt dissociation only begins at higher humidity (36% $\lesssim$ RH $\lesssim$ 46%) where sufficient water is adsorbed. These results suggest that the pre-deliquescence of sodium acetate occurs in two stages. At RH $\gtrsim$ 3%, water molecules may be found in equilibrium on the salt surface due to the effects of intermolecular forces [37, 38] acting within the system. At 36% $\lesssim$ RH $\lesssim$ 46%, enough water is adsorbed for salt solvation to occur. At this point, the presence of dissolved ions within the adsorbed film shifts the system equilibrium [98] allowing the stability of thicker adsorbed films.

Second, a sodium depletion is observed at the salt surface after completing a deliquescence/efflorescence cycle. This is explained by the recombination of the CH_3COO^- ions with H^+ to form acetic acid (CH_3COOH) upon salt dissociation. As CH_3COOH has a higher surface propensity than the sodium and acetate ions [89], an enrichment of acetic acid at the liquid/gas interface is observed and hypothesized to remain on the salt surface upon efflorescence. These findings are especially important considering that soluble particles may undergo more deliquescence/efflorescence cycles in their airborne lifetime than previously thought. In fact, recent studies have revealed heterogeneous efflorescence pathways that can significantly shift the efflorescence point to higher humidity [28, 121].

After the interesting results obtained in **Paper II**, a similar experimental approach was undertaken for **Paper III** with the aim to study the surface behaviour of ammonium sulfate ($(NH_4)_2SO_4$), another common atmospheric salt [52], under pre-deliquescence and deliquescence conditions. Results from the APXPS measurements are presented in Fig. 2.5 showing the species observed on the sample surface at RH = 3%, RH = 48% and RH = 78% > DRH. At RH = 3%, only ammonium and sulfate ions are detected on the sample surface. Unexpected species such as S^0, HS^-, HONO, and $NH_{3(aq)}$ are identified as pre-deliquescence takes place (RH = 48%, Fig. 2.5). However, as RH is further increased above the DRH, all species vanish (even the SO_4^{2-} and NH_4^+ ions) and only S^0 is observed on the scanned surface (RH = 78%, transient, Fig. 2.5). After a relaxation time above the DRH, a steady state is found where SO_4^{2-}, NH_4^+, and NH_3 reappear and traces of HS^- and HONO are detected (RH = 78%, Fig. 2.5).

To explain the presence of these unexpected species, the following chemical reactions are suggested to take place within the pre-deliquescence layer:

$$3\,SO_4^{2-} + 4\,NH_4^+ \longrightarrow 3\,HS^- + 4\,HONO + 4\,H_2O + H^+ \tag{2.3}$$

$$2\,HONO + 2\,NH_4^+ \longrightarrow 2\,N_2 + 4\,H_2O + 2\,H^+ \tag{2.4}$$

$$3\,HS^- + 2\,HONO + 3\,H^+ \longrightarrow 3\,S^0 + N_2 + 4\,H_2O \tag{2.5}$$

$$\underline{Overall}: 3\,SO_4^{2-} + 6\,NH_4^+ \longrightarrow 3\,S^0 + N_2 + 12\,H_2O \tag{2.6}$$

A similar system of Sulfate Reducing Ammonium Oxidation (SRAO) reactions has been observed and described before to explain nitrogen depletion and sulfate reduction in anaerobic environments [34], and has been widely applied in water treatment contexts [99]. Upon pre-deliquescence, reactions 2.3, 2.4 and 2.5 may explain the presence of the observed unexpected species. It is important to note that N_2, a final product of the

SRAO mechanism, is not detected on the experimental surface. The likely explanation is that due to its high volatility, it evaporates to the gas phase. Complementary molecular dynamics simulations contributed by a collaborator verified the observations. The overall SRAO reaction is considered non spontaneous because not all of its elementary steps are thermodynamically favorable [34]. Biological catalysts such as bacteria are commonly used to facilitate the SRAO reaction in industrial settings. However, no such catalyst should be present in the system studied here. Our observations suggest that salt solvation and the interfacial nature of the pre-deliquescence system may drive the chemical mechanism. In fact at RH = 78%, although the deliquesced system is nearly saturated in sulfate and ammonium ions (reactants in reaction 2.6), no intermediate species are detected. This confirms previous findings that the SRAO mechanism does not spontaneously occur in bulk solutions [34]. The observation of this mechanism below DRH thus suggests that properties of the pre-deliquesced state may facilitate the reaction. The true nature of these properties remains uncertain and raises numerous questions regarding the implications of pre-deliquescence systems in the atmosphere.

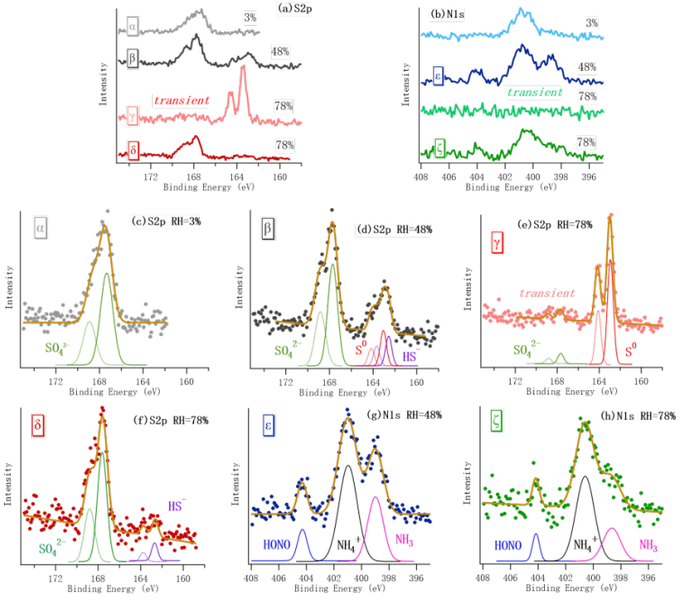

Figure 2.5: (a) S 2p and (b) N 1s XPS peaks measured at RH = 3%, RH = 48% and RH = DRH = 78%. The photon energy was set to 435 eV for sulfur XPS and 665 eV for nitrogen XPS, respectively. At RH = 3%, NH_4^+ peak and SO_4^{2-} doublet (α) were observed. At RH = 48%, S^0 and HS^- doublets (β) and HONO and NH_3 peaks (ε) appeared. At RH=78%, during deliquescence, most sulfate transferred to S^0 (γ) and no nitrogen species could be found; when deliquescence finished, the sulfur region was dominated by sulfate again (δ) and nitrogen species reappeared (ζ). Adapted from **Paper III**.

3

Ice Nucleation and PINCii

In case of fire,

- *When the fire alarm goes off - start the evacuation immediately!*
- *Look around and follow the green signs for evacuation. Always pick the nearest escape route.*
- *Assist others that are in obvious danger, as long as you do not expose yourself to risks. Remember that fire smoke is toxic - get out safely by crawling along the floor. Close all windows and doors.*
- *Warn others that may not perceive the alarm.*
- *Call the emergency number 112 and alert the emergency services - do not forget to specify the location of the fire.*
- *Extinguish the fire if possible but without taking unnecessary risks. Fire extinguishers are deployed at strategic locations and are marked out in the evacuation plan...*

University of Gothenburg, Fire procedure.

Contents

3.1 Background

The global average fraction of the ice phase represents ≈ 65-70% of the total cloud water content over the planet [115, 116] and thus plays a key role in the influence of clouds on global scale processes such as the water cycle, the radiative budget of the planet and atmospheric chemistry. The ice phase is particularly important within high level clouds (T ≤ -37°C) where water droplets homogeneously freeze. It may also represent a significant fraction of the water content of mid-level clouds (0 ≤ T < -37°C) depending on multiplication processes [35, 85, 133] and the availability of INPs that trigger ice nucleation. Although the characteristics of good CCNs are generally well known [70], the intrinsic properties of INPs have been a long missing puzzle piece. For many years, it was thought that heterogeneous ice nucleation is stimulated by surfaces that effectively template the hexagonal structure of ice. Silver iodide is a prominent example that has been commonly used for cloud seeding experiments [125]. However, it has become clear that a range of particle characteristics can influence and potentially enhance heterogeneous ice nucleation [56]. For example, biological particles and especially some types of bacteria possess proteins that stimulate nucleation near 0°C [83]. Likewise, biological macromolecules originating from pollen grains can trigger nucleation below ≈ -17°C [3, 96]. Electron microscopy has revealed that surface defects on K-feldspar rich mineral dust trigger nucleation [59] and other heterogeneities on particle surfaces such as pores may also play a role and enhance water condensation and freezing by creating convex interfaces [27, 77]. Furthermore, particle surface attributes that make ice nucleation possible may vary as a function of environmental conditions and some particles may therefore only act as INPs for a certain range of RH and T conditions. For example mineral dust particles, acknowledged as important INPs [56] because of their availability in the atmosphere [117] and their strong ice nucleation ability [50] may start triggering ice nucleation at T $\lesssim -10$°C and are therefore relevant in the formation of most mid-level clouds [56]. Soot particles which only act as INPs at T $\lesssim -23$°C, likely have little importance in ice nucleation processes at T $\gtrsim -23$°C but may play key roles in ice crystals formation at colder temperatures where their ability to act as INPs is greater [76].

With these knowledge gaps in mind, the aspiration to identify and quantify atmospheric INPs as a function of environmental conditions has driven the development of different types of ice nucleation instruments since the 1940's. These include cloud chambers [2, 79], filter sampling and nucleation testing methods [16, 23, 48, 69, 93, 103, 106, 114] and flow reactors, including Continuous Flow Diffusion Chambers (CFDCs). The first CFDCs were

developed in the 1980s and featured a cylindrical design [53, 100] and in 2008 the Zurich Ice Nucleation Chamber (ZINC) was developed [112], which was the first parallel-plate CFDC.

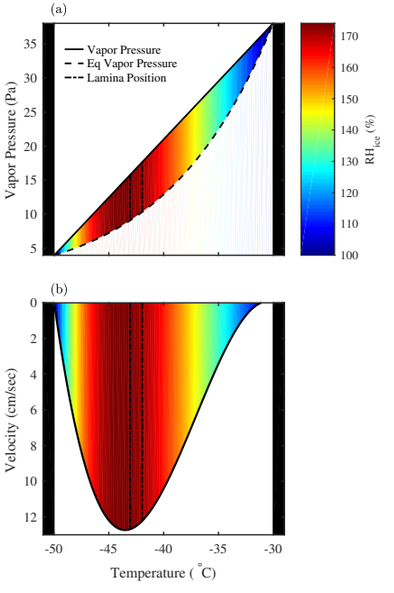

Figure 3.1: Idealized representation of the thermodynamic and flow conditions between the walls of a parallel-place CFDC assuming that the cold wall (left) is fixed at T = -50°C and the warm wall (right) at T = -30°C and a 1 cm gap separates the walls. In the top panel (a) the linear gradient of vapor pressure (solid line) is plotted with a dashed line representing the theoretical equilibrium vapor pressure over ice. The sample lamina position (within the dashed-dotted lines) is depicted in both panels as is the predicted main chamber RH_{ice}, as visualized with the color-map. The bottom panel (b) displays the flow velocity profile (solid line). Reproduced from **Paper V**.

Parallel-plate CFDCs are flow chambers wherein atmospheric conditions are reproduced by setting a specific T and RH. A flow containing sampled particles is injected into the chamber where particles may (or may not) trigger ice crystal formation depending on their capacity to act as INPs at the set T and RH conditions. Ice crystals are then counted upon exiting the chamber and the number of measured ice crystals is assumed equal to the number of INPs initially present in the sampled particle population. When brought to the field, CFDCs can provide online measurements of the INP concentrations of passing air masses and in the laboratory they can be used to study the ice nucleation potential of laboratory created particles at given conditions. To accomplish this, all parallel-plate CFDCs follow a common working principle in which a thin lamina of air containing the sampled particles (region within the dashed-dotted lines, Fig. 3.1) is sandwiched between dry and clean air and the whole flows through a chamber that is held at sub-zero temperatures and has flat and parallel ice coated walls (black shading, Fig. 3.1). The ice coating is built prior to experiments by filling the chamber with refrigerated (and deionized) liquid water while the chamber walls (made of a material facilitating ice formation) are kept below 0°C. After some residence time given for liquid water to freeze on the chamber walls, the remaining liquid is evacuated thus

leaving the chamber walls with a thin ice coating. This ice coating provides water vapour in the chamber (solid line, Fig. 3.1(a)) via sublimation and maintains a vapor pressure at the ice/gas interfaces that is equal to the equilibrium vapor pressure of ice (dashed line, Fig. 3.1(a)) for the set wall temperatures ($p = p_{ice}(T)$ at the ice/gas interfaces in Fig. 3.1). By setting a temperature gradient between the walls, a linear vapour pressure gradient is imposed between the ice layers that maintain their respective equilibrium. Because of the exponential relationship between T and p_{ice} [20, 21, 100], the imposed vapour pressure exceeds the theoretical equilibrium vapour pressure across the chamber and supersaturation with respect to ice is created (colorbar, Fig. 3.1). Because particles travel through the main chamber within a thin lamina of air, they are exposed to a narrow range of temperature and humidity conditions (T_{lam} and RH_{lam}) that can be chosen by setting the wall temperatures. Because the equilibrium vapour pressure of ice is lower than the equilibrium vapor pressure of liquid water at the same temperature [20, 21], the supersaturation-driven growth of hydrometeors results in faster and more growth of ice crystals compared to liquid droplets. CFDCs may also have an evaporation section, placed downstream and thermally insulated from the main chamber, where the walls are kept at isothermal conditions to make water vapor saturated with respect to ice ($RH_{ice} = 100\%$) but sub-saturated with respect to liquid water ($RH_{liq} < 100\%$). Thus, while travelling through the evaporation section, any liquid droplets are evaporated, while ice particles remain at equilibrium. Evaporation sections thus amplify the size differences, and ice crystals may thus be differentiated from other particles by light scattering or polarization [39, 87] and counted upon exiting the chamber [53]. The number and character of INPs can be compared to the input sample using a host of aerosol characterization instrumentation.

After the success of the parallel-plate CFDC ZINC, a portable version, the Portable Ice Nucleation Chamber (PINC) [19] was developed in late 2000's for use in remote locations and on airplane measurement campaigns. Simultaneously, horizontal designs such as the the Horizontal Ice Nucleation Chamber (HINC) [55, 68] were developed to improve on limitations of the vertical design. Subsequently, commercialized vertical chambers like the Droplet Measurement Technology SPIN chamber [39] and the CFDC-IAS (Handix Scientific, Boulder, Colorado, USA) have been produced. Most recently, a new horizontal chamber able to operate autonomously was developed (HINC-auto) [11] and has now been operating continuously at the Jungfraujoch (Switzerland) for two years. Considering the current wealth of available ice nucleation chambers, it may seem surprising that new methods emerge. However, the method employed by parallel-plate CFDCs comes with a number of uncertainties such as (i) the potential break away of ice crystals from the ice-coated walls that can contaminate crystal counts from nucleated INPs; (ii) the deviation of sampled particles from the expected lamina conditions; (iii) the high sensitivity to the

wall temperatures of lamina conditions, resulting in uncertainties within the conditions to which particles are exposed. These limitations push the development of better technologies and the Portable Ice Nucleation Chamber II (PINCii) is a new parallel-plate CFDC that has been an ongoing focus of development throughout my PhD.

3.2 PINCii development and the HyICE campaign

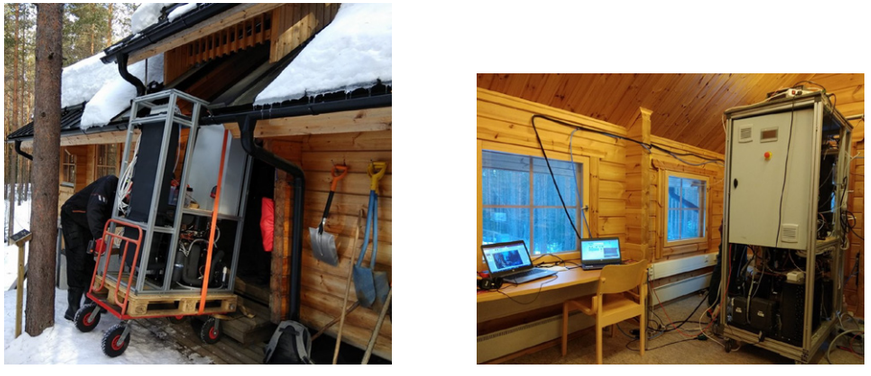

Figure 3.2: Photos of PINCii's first deployment to Hyytiälä (Finland) in 2018.

PINCii is the product of a six partner technology agreement including the University of Helsinki, TROPOS, ETH-Zurich, Aarhus University, Lund University and the University of Gothenburg. The development of PINCii was largely initiated and managed in Göteborg (Sweden) by the University of Gothenburg which partnered with the refrigeration design firm NR-KYL located nearby. By August 2016 when my PhD studies began, the first PINCii prototype was assembled and being tested. This first unit suffered from serious deficiencies. First, it was far from vacuum tight and strong cooling cycles quickly opened larger water leaks. Furthermore, the refrigeration system did not cool the chamber walls uniformly and the software could only control the main chamber functions. To fix the leak issues chamber parts were re-engineered and a new o-rings chamber fastening was implemented to uniformly seal the different chamber parts together. Furthermore, several iterations of

the the cooling system were designed in order to find a working balance between cooling power and cooling uniformity along the chamber walls.

In 2018 an unfinished version of the PINCii was brought to the Station for Measuring Ecosystem Atmosphere Relations (SMEAR) II at Hyytiälä (Finland) with the aim to finalize the instrument on site and take part in the HyICE-2018 field campaign. Photographs of PINCii's deployment to SMEAR II are presented in Fig. 3.2. The SMEAR II station [25, 45] is in the boreal coniferous forest and remotely located away from large anthropogenic emissions and dust sources which are usually considered common INP sources [56]. Considering the wealth of aerosol and meteorological variables continuously being monitored at the SMEAR II station [25, 45], it is an ideal measurement site to use as a proxy for characterizing the boreal forest environment which represents more than one-third of all forests [120]. The HyICE-2018 campaign thus gathered various types of ice nucleation chambers [19, 39, 82] and offline methods [48, 93, 103], for which contributions to the campaign are summarized in Fig. 3.3. The primary objective of HyICE-2018 was to improve knowledge with respect to the sources and concentrations of INPs in the boreal environment. This objective was successfully accomplished and several publications have resulted from the campaign. For example, showing the long range sources of INPs in Hyytiälä [90] and the predictable INP concentrations on a seasonal scale [104]. The secondary objective of HyICE-2018 was to use the gathering of various ice nucleation instruments to inter-compare their measurements in a field setting. For this purpose, four days were selected March 22nd, March 28th, April 26th and April 28th of 2018 (dashed lines, Fig. 3.3). During these inter-comparisons, the various research groups aimed to measure simultaneously at similar experimental conditions (T = -32°C, RH_{liq} = 105%). For the initial two days, PINCii was still under development and unable to take part to the inter-comparisons. PINCii started measuring on April 22nd and continued on a daily basis (5+ hours per day) until June 10th, the end-date of the campaign. The total collected data can be visualized in Fig. 3.4 and the results showed INP concentrations in the same order of magnitude as what the other ice nucleation chambers present on site measured [10].

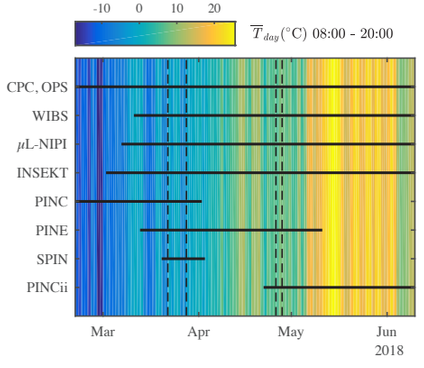

Figure 3.3: Timeline of deployment for various particle counters and INP counting instrumentation specifically added to augment the SMEAR II capabilities during HyICE-2018. Shading depicts mean daytime air temperature averaged between 08:00–20:00 (UTC+2) measured at 4.2 m height for the campaign period. Instrument inter-comparison days are indicated by the dashed lines. Reproduced from **Paper IV**.

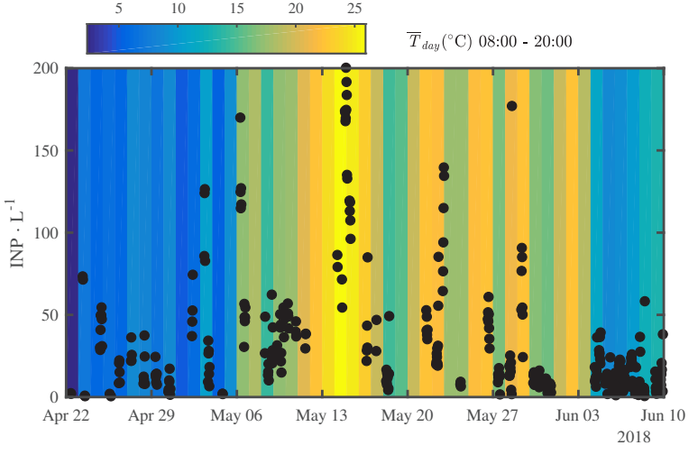

Figure 3.4: INP concentrations measured by PINCii between April 22nd and June 10th with T_{lam} = -32°C, $RH_{liq,lam}$ = 105%. Data points represent 15 min averages of sampling intervals separated by 15 min background measurements of filtered air. The background colormap represents the daytime air temperature averaged between 08:00 – 20:00 (UTC+2) measured at 4.2 m height

PINCii did take part in the last two inter-comparison days, measuring side-by-side with the PINE chamber [82]. PINE and PINCii measured consistent INP concentrations within the same order of magnitude and observed similar trends throughout the days, as presented in Figs. 11 & 12, **Paper IV**.

Overall, PINCii's measurements in Hyytiälä showed that although the instrument was newly built, its performance was comparable to well evaluated ice nucleation chambers [10, 19, 39]. Subsequent to HyICE-2018, PINCii was kept in Hyytiälä to collect additional data. On June 12th, a power loss disconnected the instrument from its control computer resulting in excess heating. PINCii burnt. A photo showing the damage to the chamber is shown in Fig. 3.5. The system was returned to Gothenurg, re-built, and improved on some limitations that were identified during its operation in Hyytiälä. A safety system was also added to the set-up. Once finalized the new iteration was sent to the european organization for nuclear research (CERN) in Geneva (Switzerland) where it could perform

further instrumental comparisons. However, on its way to CERN, a shipping accident displaced chamber parts and resulted in significant leak issues. The chamber was once again entierely re-built adopting yet more engineering refinements. To the design in order to improve the chamber tightness and to the software to improve the temperature control. This latest iteration of the PINCii instrument is the result of lessons learnt throughout five years of development. Although improvements can still be implemented, it is considered to be the reproducible PINCii package. This iteration was evaluated through numerous calibration/testing experiments and **Paper V** presents its design, capabilities, evaluation and uncertainty assessment.

Figure 3.5: Photo of PINCii's main chamber coming back from Hyytälä.

3.3 The Portable Ice Nucleation Chamber II - PINCii

PINCii follows the same working principal as the previous generations of parallel-plate CFDCs previously described in § 3.1. The instrument was however initially constructed with an upgraded design and temperature control in order to respond to some common limitations from previous parallel-plate CFDCs. Further upgrades also emerged during the development process such as an updated thermodynamic model used to calculate the chamber conditions, the possibility to use PINCii as a low temperature Cloud Condensation Nuclei (CCN) counter and new ways of analyzing ice nucleation data to account for the T_{lam} and RH_{lam} uncertainties to which particles are exposed while flowing through the chamber.

3.3.1 Design

The whole PINCii package is a transportable instrument that can be moved for field sampling but requires a three-phase power source. PINCii weighs ≈ 400 kg and is mounted on a transportable rack of ≈ 0.8 × 1.2 × 2 m outer dimensions that can be shipped on a standard

wooden pallet. This includes a refrigeration system, an electrical cabinet, the experimental chamber as well as external devices such as mass flow controllers, filters, dryers, tubing, control computer etc.

The experimental chamber is constructed of aluminium to ensure good portability and thermal conductivity. The inner parts are sandblasted and anodized to facilitate freezing and cohesion of ice on the chamber walls. Details of the experimental chamber design and dimensions are presented in Fig. 1 from **Paper V**, where the three main sections (inlet, main chamber and evaporation section) are shown. The inlet serves to inject the lamina flow containing the sampled particles (1 $L \cdot min^{-1}$) independently from the two sheath flows (4.5 $L \cdot min^{-1}$ each) sandwiching it. The flow values are chosen to constrain the sampled particles to a narrow range of T_{lam} and RH_{lam} conditions while travelling through the chamber. The inlet also holds a water level sensor which is used during the icing procedure to stop filling water when its level reaches the base of the aerosol inlet.

In PINCii, the main chamber, where supersaturated conditions are created for ice crystals nucleation and growth, consists of two flat parallel walls that are 33 cm wide and 1 m long and separated by a 1 cm gap. This gap is made by 1 cm thick semi-crystalline thermoplastic (SustaPEEK) sidewall pieces. The SustaPEEK material is chosen for its poor thermal conductivity and its resistance to distortions with temperature changes. With previous parallel-plate CFDCs main chambers lengths ranging from to 0.508 to 1 m for HINC[68] and SPIN[39] respectively, the PINCii 1 m main chamber maximizes the residence time of particles and enables more time for kinetically limited nucleation events and aerosol growth. This is mostly useful at cold temperatures ($T_{lam} \lesssim$ -35°C) where previous CFDC experiments have shown that ice crystals do not always reach the size threshold used for phase differentiation from water droplets, due to kinetically limited growth at such temperatures [127]. The 42 cm long evaporation section is also longer than previous CFDCs, with the SPIN's 25 cm long evaporation section [39] being the longest from earlier portable parallel-plate CFDCs. This elongated evaporation section gives more water droplet evaporation time, which benefits the size differentiation between ice crystals and water droplets.

PINCii's temperature control is also unique. A two stage cooling system using R23 refrigerant, acting with an evaporation temperature of ≈ -72°C, can cool the chamber walls down to -67°C after losses. The coolant is injected along the chamber walls via a series of thin capillaries (Fig. 2, **Paper V**) in a similar manner to SPIN [39], in order to provide uniform cooling throughout the chamber walls. Refrigerant is injected into the main chamber and evaporation section walls via four individually controlled solenoid valves and thus each wall can be cooled separately. With the SustaPEEK flanges between the main

chamber walls, the main chamber walls can be kept at different temperatures. Although no thermal insulation is installed between the evaporation section sides, experiments have shown that a temperature gradient can also be maintained across the evaporation section. Thus the evaporation section can act as an extension of the main chamber for PINCii to operate as a low temperature CCN counter for water droplet nucleation experiments. This mode is used in **Paper V** to scan through water saturation (RH_{liq} = 100%) and the deliquescence point of sodium chloride at various temperatures (Figs. 7 & 8, **Paper V**). Refrigerant is injected into the chamber walls in pulses by opening/closing the solenoid valves and a pulse length is a function of the desired temperature set point as well as the difference between a wall temperature from its set point. In other words, cooling is strengthened to quickly cool the walls near the desired set points and the cooling is then reduced to maintain good temperature stabilization. To compensate for the cooling, silicon heating pads pairs are placed on the chamber walls (Fig. 3, **Paper V**). Each pair is individually controlled via its own PID loop to keep heating spatially flexible. The wall temperatures are monitored via a total of 58 K-type thermocouples embedded within the chamber walls and monitored at 1 Hz with a 0.1°C uncertainty. The thermocouple placement on the chamber walls is illustrated in Fig. 3, **Paper V**. The thermocouple monitoring is continuously used as an input to the cooling and the heating system in order to provide cooling/heating where and when it is required. Thermocouples data is also recorded to calculate the lamina conditions to which particles are exposed, using the thermodynamic model presented next.

3.3.2 Thermodynamic Model

Thermodynamic conditions within the chamber are modelled assuming linear and equilibrated gradients between the chamber walls. To simulate the temperature, humidity and flow field in detail, including a velocity profile that accounts for buoyancy inside the chamber, a model from Rogers et al., 1988 [100] is used.

The temperature field within the chamber is represented by the one dimensional heat transfer expression [100],

$$\frac{\delta \mathrm{T}}{\delta t} = \mathrm{K}\frac{\delta^2 \mathrm{T}}{\delta \mathrm{X}^2}, \tag{3.1}$$

where T is function of both position X and time t; K represents the heat conductivity of moist air. Traditionally, Eq. 3.1 is bounded between the chamber walls temperature and

position,

$$\mathrm{T}(-w, t) = \mathrm{T_c}, \tag{3.2}$$

$$\mathrm{T}(w, t) = \mathrm{T_w}, \tag{3.3}$$

where T_c and T_w represent the warm and cold wall temperatures and w is half the separation between the walls (0.5 cm). The coordinate system is thus based at the center of the chamber. However, these boundary conditions omit the presence of ice on the chamber walls (cf. §3.1). Therefore, the thermodynamic model is updated to take into account the presence of 1 mm thick condensed ice layers on the chamber walls that reduce the total chamber volume by 20% and reduce the chamber gap from 1 cm to 0.8 cm. The ice layer thickness was estimated by measuring the volume of water coming out of the chamber after a icing/melting cycle and calculating the ice thickness assuming that this water volume was uniformly spread on the walls surfaces. The value is similar to what as been previously reported in Chou et al., 2011 [19] for the ice layer thickness of the PINC chamber. With l representing the ice layer thickness (1 mm), we define d as half the separation between the ice layers ($d = w - l$). The boundary conditions are thus modified to

$$\mathrm{T}(\text{-}d, \mathrm{t}) = \mathrm{T_{ice,c}}, \tag{3.4}$$

$$\mathrm{T}(d, \mathrm{t}) = \mathrm{T_{ice,w}}, \tag{3.5}$$

where $T_{ice,c}$ and $T_{ice,w}$ represent the temperatures at the ice/gas interfaces on the cold and warm sides of the chamber. $T_{ice,c}$ and $T_{ice,w}$ are calculated as a function of the wall temperatures by considering the heat transfer through the aluminium walls and the ice layers at steady state. That said, by assuming steady state ($\frac{\delta T}{\delta t} = 0$), Eq. 3.1 is simplified to

$$\mathrm{T(X)} = \mathrm{T_{ice,c}} + (\mathrm{T_{ice,w}} - \mathrm{T_{ice,c}}) \cdot \frac{\mathrm{X}}{2d}. \tag{3.6}$$

Eq. 3.6 thus represents a linear temperature gradient between the ice layers.

The velocity flow field equation V(Z,ΔT) is given by a parabolic velocity profile,

$$\mathrm{V(Z, \Delta T)} = \frac{3}{2}\overline{\mathrm{V}}\left(1 - \frac{\mathrm{Z}^2}{d^2}\right) + \frac{\rho_a \mathrm{U} g d^2 \Delta \mathrm{T}}{12\mu}\left[\left(\frac{\mathrm{Z}}{d}\right)^3 - \frac{\mathrm{Z}}{d}\right], \tag{3.7}$$

assuming Poiseuille flow (first term in Eq. 3.7) with an added buoyancy term [110] (last term in Eq. 3.7). In Equation 3.7, $\overline{\mathrm{V}}$ is the mean velocity, Z is the distance from the flow centerline, ρ_a is the average air density, U is the volume coefficient of expansion of air, g is the acceleration of gravity, μ is the dynamic viscosity, and ΔT the temperature gradient

imposed between the ice layers. Given a desired lamina condition, Eq. 3.7 is used directly to generate the flow velocity profile of the chamber as presented in Fig. 3.1 (b).

The lamina position is determined by integrating the velocity profile (Eq. 3.7) between the ice layers (*-d* to *d*) using unknown lamina coordinates (*a* and *b*) with an assumption of equal mass flow on either side of the lamina,

$$(1-q)\frac{\mathrm{Q}}{2} = \frac{\mathrm{Q}}{2d\overline{\mathrm{V}}}\int_{-d}^{a}\mathrm{V(Z,\Delta T)dZ} = \frac{\mathrm{Q}}{2d\overline{\mathrm{V}}}\int_{b}^{d}\mathrm{V(Z,\Delta T)dZ}. \tag{3.8}$$

Here Q is the total volume flow rate and q is the fraction of total flow that is found in the lamina. The result of Equation 3.8 is a fourth order polynomial equation,

$$-\frac{\rho_{\mathrm{a}}\mathrm{Ug}\Delta\mathrm{T}}{48\mu d^2\overline{\mathrm{V}}}b^4 + \frac{1}{2d^3}b^3 + \frac{\rho_{\mathrm{a}}\mathrm{Ug}\Delta\mathrm{T}}{24\mu\overline{\mathrm{V}}}b^2 - \frac{3}{2d}b + 1 - \frac{\rho_{\mathrm{a}}\mathrm{U}g\,d^2\Delta\mathrm{T}}{48\mu\overline{\mathrm{V}}} - (1-q) = 0, \tag{3.9}$$

where the roots *a, b* can be extracted using a computational root finding algorithm.

Accounting for the presence of the ice layers within the thermodynamic model influences the calculated lamina conditions to which particles are exposed as well as the velocity profile across the chamber. The presence of backflow presented in Garimella et al., 2016 [39] is no longer found to be important with this new calculation as represented in Figs. 5 & 6, **Paper V**.

The current model assumes that ice is homogeneously spread on the walls. However, this is unlikely. During icing of the chamber walls, water is injected from the bottom (Fig. 3.7), once the chamber is filled, the water pump stops for 5 sec before reversing its direction and emptying the chamber via the bottom. The complete process takes ≈ 45 sec with the chamber top being exposed to water for 5 sec and the bottom for ≈ 45 sec. This discrepancy in exposure times between the chamber top and bottom should inevitably result in thicker ice layers towards the chamber bottom. However, the ice layer thickness as a function of the chamber height is challenging to measure. Because the main chamber and the evaporation section are thermally insulated from one another (Fig. 1, **Paper V**), a melting of the evaporation section can be done prior to the melting of the main chamber thus returning an average ice layer thickness for the evaporation section and an average thickness for the main chamber. Furthermore, since the water is filled/emptied at a constant rate (flow rate of the water pump), a linear relationship of the ice layer thickness with chamber height can be assumed. Bringing this information together and calculating the slope of this linear

relationship so that the ice layer thickness at the main chamber bottom matches the ice layer thickness at the evaporation section top, an ice layer thickness profile can be estimated as presented in Fig. 3.6 where the black shadings represents the ice layers. Fig. 3.6 also shows temperature, saturation, and velocity fields calculated using the thermodynamic model presented above. In this example, the lamina conditions are $\mathrm{T_{lam}}$ = -32°C and $\mathrm{RH_{liq,lam}}$ = 105% which were the experimental conditions used during the HyICE-2018 field campaign [10]. However, this method to estimate the ice layer thickness profile does not account for secondary effects like latent heat release during freezing. Without more evidence, implementing this method may introduce more uncertainties than it solves. Therefore, the ice layer thickness is assumed to be 1 mm over the entire wall surface in the results presented in **Paper V**.

3.3.3 Operation

In order to operate the PINCii instrument, an array of external devices such as pumps, mass flow controllers (MFCs), filters, atomizer, Differential Mobility Analyzer (DMA), Condensation Particle Counters (CPCs), Optical Particle Counter (OPC), etc. are required. A schematic of the system used for the experiments performed for **Paper V** is presented in Fig. 3.7. Sheath flow is supplied from a nitrogen or compressed air source that is filtered, dried and cooled. The flow is cooled by travelling through a copper pipe placed within the insulation material near the cold main chamber wall. The sheath flow is then divided and regulated via two MFCs before being injected into the chamber. When used in a laboratory setting, this cooled, cleaned and dried air is also passed through a particle generator (e.g., atomizer) and DMA before being connected to the sample flow inlet port as shown in Fig. 3.7. When used in the field, the sample flow inlet port is directly connected to ambient air with a size cutoff selector (e.g., impactor) to remove the largest particle fraction that may be difficult to differentiate from nucleated ice crystals. A solenoid valve is also attached to the sample flow inlet port. It is used to alternate between a sampling line containing the particles and a filtered line used to measure the background concentration of ice crystals being dislodged from the ice coated walls. At the bottom of the chamber, a water pump can be attached to perform the ice coating procedure of the chamber walls prior to experiments. After the icing procedure, the water line is manually replaced by an OPC to measure the outgoing aerosol concentration as a function of particle size. For the experiments presented in **Paper V**, a four size Channel (Ch) OPC (Remote 3104, Lighthouse Worldwide Solutions, USA) is used. With $\mathrm{d_p}$ used to signify the particle diameter, the four OPC size channels are

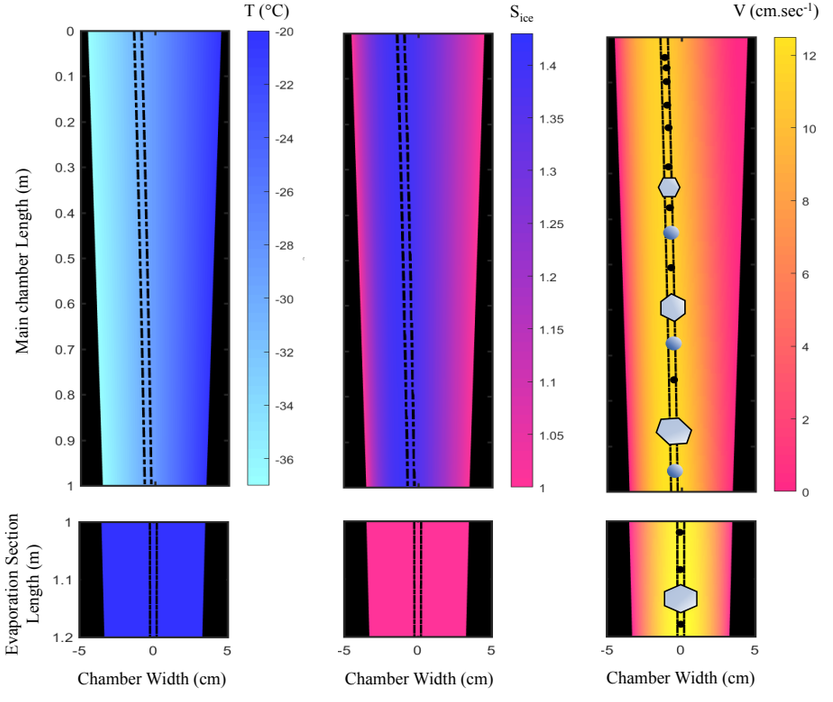

Figure 3.6: Temperature, saturation with respect to ice (S_{ice}), velocity, and lamina conditions across the main chamber and evaporation section. These variables are calculated using the thermodynamic model presented in § 3.3.2 assuming a linear decrease of the ice layer thickness (black shading) with chamber height. The average thickness of an ice layer is 1mm. Lamina position is represented by dahed-dotted lines. Hydrometeors nucleation and growth is also illustrated. Hydrometeors nucleate and grow in the main chamber and water droplets evaporate in the evaporation section. The wall temperatures chosen for this simulation were calculated to represent the lamina conditions (T_{lam} = -32°C and $RH_{liq,lam}$ = 105%) used during the HyICE campaign (e.g., Fig. 3.4).

: $0.3 \leq d_p < 1$ µm; $1 \leq d_p < 3$ µm; $3 \leq d_p < 5$ µm; and $d_p \geq 5$ µm. For the purpose of data analysis and visualisation these size bins are cumulatively combined in Ch1: $d_p \geq 0.3$ µm; Ch2: $d_p \geq 1$ µm; Ch3: $d_p \geq 3$ µm; Ch4: $d_p \geq 5$ µm.

Before each experiment and prior to the icing procedure, the chamber is cleaned by injecting sheath flow via the two MFCs respectively set at 4.5 $L \cdot min^{-1}$. During that purge, the main chamber walls are cooled to -23°C and the evaporation section walls to -20°C. These are

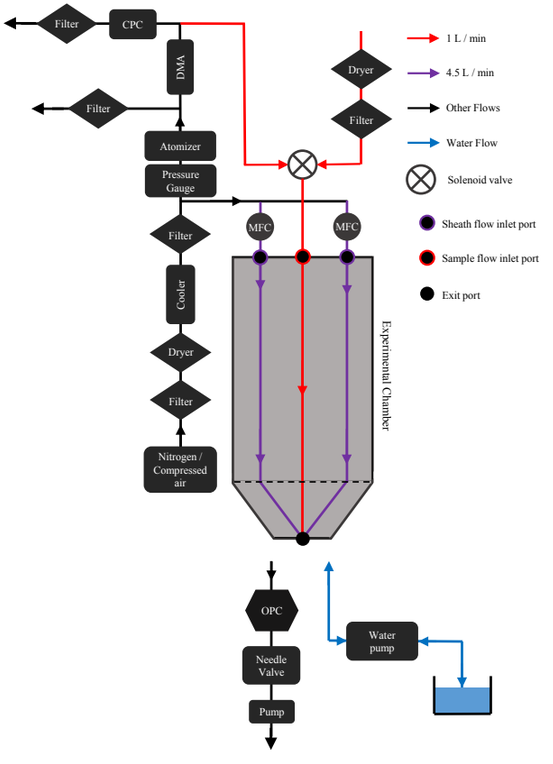

Figure 3.7: Schematic of the experimental set-up used for the experiments performed in **Paper V** describing the air and water flow diagrams outside of the experimental chamber. Clean, dried and cooled flows of compressed air are regulated at 4.5 $L \cdot min^{-1}$ by two MFCs and injected into to the chamber via the sheath flow inlet ports to create the chamber sheath flows. Through the sample flow inlet port dried and filtered air or a flow containing the sampled particles is injected depending on the position of the labview-controlled solenoid valve. In the majority of the experiments performed for **Paper V**, particles are dispersed via an atomizer, size-selected via a DMA and counted with CPC before being injected into the chamber. At the outlet, the OPC is used to measure the activated aerosol concentration exiting the chamber. Air is pulled into the chamber by a pump placed downstream of the OPC and a needle valve is used to set the total pulled flow to 10 $L \cdot min^{-1}$. Prior to experiments, a water line consisting of a pump and water reservoir is attached at the outlet to execute the ice coating procedure. The power and direction of the water pump are controlled via the connected computer.

the wall temperatures set prior to the icing of the chamber walls. The evaporation section is 3°C warmer than the main chamber in order to compensate for the longer exposure time to water and to prevent the formation of too thick ice layers towards the chamber bottom. Although these temperatures are arbitrarily chosen, they are the result of much trial and error that have led to good stability of the ice layers and a low background signal. Once a stable temperature is reached, the sheath flow is stopped, the user verifies that the inlet valve is in filter mode and the water pump is attached. The water filling program is initiated to activate the water pump and fill the chamber with refrigerated (1 to 5°C), deionized water until the water level sensor located at the inlet base is reached, stopping the water pump. After a 5 sec delay for freezing, the pump direction is reversed and the chamber is emptied of any remaining liquid. After 200 sec of evacuating the liquid water, the pump stops and is manually detached from the exit. After removing the pump, the exit is dried and 9 $L \cdot min^{-1}$ of sheath flow is injected into the chamber, in order to sublimate structural heterogeneities from the newly formed ice surfaces. The latent heat released during freezing warms the walls up to ≈ 0°C. The walls are immediately cooled to -5°C and once stable at this temperature, the walls are cooled in a step-wise manner by 5°C increments ensuring temperature stabilization at each step. The step-wise cooling of the chamber walls is to ensure ice layer stability because fast cooling rates have been shown through numerous experiments to result in higher background values. Once the desired wall temperatures are achieved, the exit is once again dried and the OPC is attached. The pump downstream of the OPC is turned on and the needle valve adjusted to achieve 10 $L \cdot min^{-1}$ total flow exiting the chamber. When the procedure is successfully followed, background counts near $0 \cdot L^{-1}$ are achieved in all size channels.

Several measurement modes have been implemented within the software and the user can benefit from the flexibility of the PINCii instrument. In standard mode, the wall temperatures are kept constant and the inlet solenoid valve is switched at a desired frequency to alternate sampling and background intervals. This mode is most relevant in a field setting to measure the INP concentration of a passing air mass at given T_{lam}/RH_{lam} conditions as shown in Fig. 3.4. It has also been used to perform the background measurements presented in Fig. 13, **Paper V**. The chamber can also operate in a ramping mode where RH_{lam} is incrementally increased at $1\% \cdot min^{-1}$ within a desired RH_{lam} interval for a given T_{lam}. This mode has been used to perform all the activation experiments described in **Paper V**. PINCii can also be used as a cold temperature CCN counter by maintaining a temperature gradient in the evaporation section, which thus acts as an extension of the main chamber for hydrometeors to grow. This has been used to perform droplet nucleation and deliquescence experiments presented in Figs. 7 & 8, **Paper V**.

3.3.4 Experimental Results

The main test for any new instrument is to evaluate its performance in a well constrained manner against reliable predictions. When it comes to ice nucleation, the evaluation possibilities are rather limited. In fact, no theory is yet able to reliably predict the nucleating conditions of given particles and inter-instrumental comparisons come with added uncertainty. The only references that can be used within the reachable temperature conditions of the PINCii instrument (-55°C < T_{lam} < -5°C) are the homogeneous freezing onset of pure water at T ≈ -37°C, RH_{liq} = 100% [64, 86] and the homogeneous freezing of solutions described by Koop theory [64]. Although these are the references for ice nucleation, previous instruments have consistently shown deviations from the predictions as summarized in Welti et al., 2020 [127]. These deviations have partly been attributed to kinetically limited ice crystal growth at cold temperatures [105, 127] and to instrumental uncertainties.

Paper V shows that similar deviations from the Koop theory were initially observed but these deviations could be explained and corrected by considering kinetically limited ice crystals growth [105, 127] as well as the non-reversible characteristic of ice nucleation (Fig. 10, **Paper V**). Welti et al., 2020 [127] showed that kinetically limited ice crystals growth becomes an issue for the SPIN chamber in the homogeneous freezing regime because ice crystals may not grow large enough to be detectable in the OPC size threshold assigned to their detection. Such observations are confirmed in our experiments where ice crystals are not detected in the $d_p \geq 5\mu m$ size bin but can be observed if the threshold is lowered to 3 μm (Fig. 10 (b), **Paper V**). However, this artifact alone does not completely explain the deviations from the Koop theory and **Paper V** shows that the other part of the problem lays within T_{lam}/RH_{lam} uncertainties to which particles are exposed when travelling through the chamber. In fact, because homogeneous freezing is a nucleation process occurring well above the equilibrium vapour pressure of the created ice phase (see position of the homogeneous freezing onset in Fig. 6 from **Paper V** or in Fig. 3.9 below), it is not reversible. If the sampled particles are exposed to T_{lam}/RH_{lam} anomalies that may trigger their activation to ice crystals, the formed ice crystals will keep growing in the chamber even if they are further exposed to conditions well below their activation onset.

This is shown in Fig. 3.8, where the homogeneous freezing of a natural salt sample collected in the Qaidam basin (China) and size selected at 200 nm is presented. In panel (a), the ice crystal concentration emerging from the chamber is presented in a conventional way against the average lamina conditions recorded inside the chamber, with the size threshold

for detecting ice crystals set at 3 μm in order to account for kinetically limited ice crystals growth. This method of treating data results in an observed homogeneous freezing onset below the theoretical prediction [64]. When zooming into the first data point exceeding the background concentration (circled data point) and thus capturing the first homogeneous freezing onset record at T_{lam} = -50°C, panel (b) shows the spread in the lamina conditions to which particles were exposed while travelling through the main chamber. This spread represents the lamina uncertainties for this specific data point and shows that particles were exposed to T/RH conditions above the theoretical homogeneous freezing onset (data point above the dashed line in panel (b)) and that this one anomaly may be responsible for the observed freezing. In panel (c), a vector analysis is performed so that for every OPC record, the various lamina conditions measured along the chamber are analyzed in order to identify the condition most likely to have triggered nucleation (closest point from the Koop line if all data points are below it and the furthest above the Koop line if one or more data points are measured above it). When the ice crystals counts are plotted against the extreme lamina conditions recorded (c) rather than the average (a), a much better fit to the homogeneous freezing onset is found. This method of analyzing ice nucleation data was confirmed using two natural salt samples from the Qaidam basin and two sodium chloride duplicates (Fig. 3.9).

The PINCii was also evaluated with respect to heterogeneous freezing, deliquescence and droplet nucleation in order to evaluate its capabilities over the entire range of achievable T_{lam}/RH_{lam} conditions (Fig. 6 from **Paper V**). The recorded onsets of these nucleation processes are summarized in Fig. 3.9 and compared to their predictions. All the results are in very good agreement to their respective predictions, thus showing the reliability of the PINCii instrument. The main uncertainties (background, particle loss and lamina conditions) were also assessed and quantified. It was shown that PINCii can maintain background concentrations ≤ 0.12counts $\cdot L^{-1}$ for 5.5 h under strong forcing conditions (T_{lam} = -50°C and $RH_{ice,lam}$ = 155%). These background values are significantly lower than those reported from previous chambers [19] and largely the result of the very specific icing method presented in § 3.3.3. Whether or not this method is applicable to other CFDCs remains uncertain but it is clear that PINCii is an instrument well suited to sample in environments with low INP concentrations. The instrument showed negligible particle loss (e.g., Fig. 14 from **Paper V**) and the lamina spread was estimated around 9% using the strongest relevant temperature gradient. The uncertainties in T_{lam} and RH_{lam} recorded during the droplet nucleation, homogeneous freezing and particle loss experiments are presented in Fig. 16, **Paper V**.

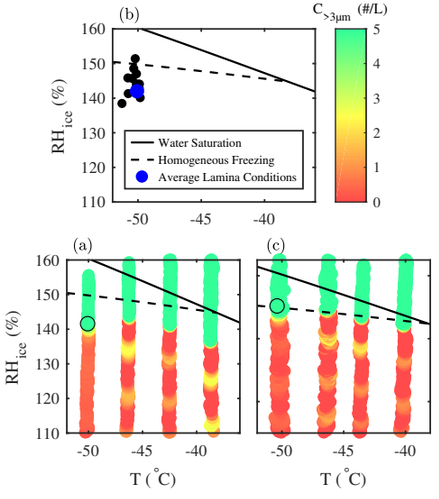

Figure 3.8: In Panel (a) the concentration of aerosols > 3 μm observed to exit the chamber is plotted against the average temperature and humidity conditions measured along the lamina. Panel (b) shows the details of the first data point exceeding 5 counts $\cdot L^{-1}$ at T ≈ -50°C where all the measured lamina conditions are plotted as individual data points on the phase diagram thus showing the various conditions to which particles are exposed while travelling along the lamina. Panel (c) presents the same data as Panel (a) but showing aerosol concentration against the extreme lamina conditions that particles travelled through rather than the average. Extreme conditions are determined by doing a vector analysis to identify the data point closest to the Koop line if all data points are found below the Koop line or identifying the data point furthest above the Koop line if several data points are recorded above it.

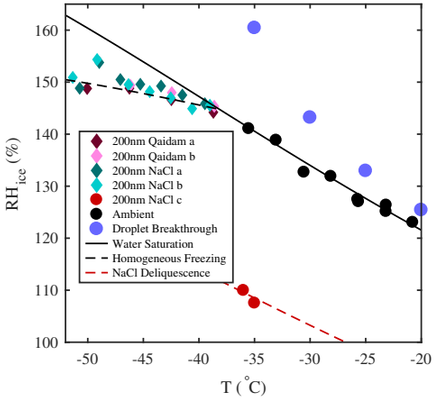

Figure 3.9: Summary of the activation onsets measured in the droplet nucleation, homogeneous freezing, deliquescence and droplet breakthrough experiments. Activation onsets are defined as concentrations or activated fractions exceeding background levels. Reproduced from **Paper V**.

4

Implications and Future Perspectives

"I have not failed. I have successfully discovered 10 000 things that will not work."

Thomas Edison.

Contents

4.1 Pre-Deliquescence

The first part of this thesis has presented a pre-deliquescence theory and its capacity to represent hygroscopicity measurements of NaCl particles using a set of physically realistic parameters. This suggests that the adsorption of water layers on soluble particles may be the result of a combination of dissolved ions, and intermolecular forces which in sum permit the meta-stability of the observed condensed water. As the theory is currently presented, it leaves three parameters (surface charge, hamaker constant and layer concentration) as free parameters to match experimental observations. As shown in Figure 2.3, the layer concentration can be parameterized as a function of particle size, thus leaving the possibility to constrain surface charge and hamaker constant in order to present a theory that will be able to not only reproduce but also predict the hygroscopicity of given compounds. The use of such an equation could thus be found in the simulation of pre-deliquescence systems within atmospheric modelling.

The pre-deliquescence theory has only been tested for a pure NaCl system, further studies could extend the theory to other pure salts and maybe to mixed-inorganic systems and/or account for the presence of organics within the mixture. This will render the theory more representative of atmospheric particulate. This theory may also have implications within the persistence of arctic mixed phase clouds and the suggested extension to the WBF process may partially explain the longevity of the liquid phase within certain scenarios. A more comprehensive study experimentally showing the diffusion of water vapor from the ice to pre-deliquesced particles and constraining the T/RH conditions where this process may be relevant would make light on the potential of the given hypothesis.

Experimental observations using the APXPS method have revealed chemical and physical processes taking place on the surface of pre-deliquesced salts. A sodium depletion is observed on the surface of a sodium acetate sample after completing a deliquescence/efflorenscence cycle. This depletion is attributed to a formation of acetic acid and its selective enrichment to the liquid/gas interface. Furthermore, novel chemistry is observed at the surface of an ammonium sulfate sample whereby numerous intermediate species are observed. We also show that the chemical mechanism responsible to the formation of the observed species is facilitated within the pre-deliquesced film. Given the abundance of sodium acetate and ammonium sulfate in the atmosphere and the wide RH range where pre-deliquescesced particles can be found, these findings may have important atmospheric chemistry implications.

4.2 Ice Nucleation and PINCii

This second theme has presented the development of the new Portable Ice Nucleation Chamber II - PINCii and evaluated its latest iteration. I have shown that the PINCii chamber successfully reproduces droplet formation, deliquescence, homogeneous and heterogeneous freezing processes with very good accuracy.

I also showed that consistent deviations observed between the Koop theory [64] and experimental data [105, 127] may be understood by accounting for the temperature anomalies found along the chamber walls. Homogeneous freezing occurs well above the equilibrium vapor pressure of ice. Therefore newly frozen droplets are found in a strongly supersaturated environment and quickly grow in size. In the chamber, if T_{lam}/RH_{lam} anomalies trigger homogeneous freezing, the formed crystals will keep growing whether or not they are further exposed to T_{lam}/RH_{lam} conditions beyond the homogeneous freezing onset. When plotting observed nucleated ice crystals counts against the extreme lamina conditions rather than the conventional average measured throughout the chamber, data showed a much better agreement with the homogeneous freezing onset.

These findings also bring to light the potentially biased way ice nucleation data is currently treated within the community. I suggest that this bias is applicable not only to homogeneous freezing but to most CFDC experiments. In fact, ice nucleation, whether it is homogeneous freezing, deposition freezing, immersion freezing, contact freezing etc. is a non-reversible process occurring in strongly super-saturated conditions with respect to ice. This hints that other ice nucleation measurements may be subject to the same bias. This is however hard to prove because ice nucleation is currently not well constrained and unlike homogeneous freezing which is well represented through the Koop theory [64], heterogeneous processes do not have clear theoretical representations.

The main uncertainties of the chamber were also addressed while showing PINCii's low background signal compared to its predecessors. This benefit makes it an instrument of choice to measure in environments with low INP concentrations.

4.3 Concluding Remarks

This thesis work has tried to shed light on molecular level processes related to the physics and chemistry of atmospheric aerosols. We suggested a simple thermodynamic model able to explain and capture the evolution of pure salt particles in the atmosphere. If better constrained and extended to represent relevant atmospheric particle compositions, this model may have the potential to be implemented within atmospheric models to represent the equilibrium state of soluble particles with changing environmental conditions. We have also shown that the pre-deliquescence state can be a medium for aqueous chemistry and can facilitate certain chemical reactions. Given that soluble particles are the second most abundant aerosol particle species [71] and that pre-deliquescence can cover a very wide range of RH/T conditions [14], these findings may have implications in the way atmospheric surface chemistry is treated. Finally, we have developed the PINCii instrument. A new ice nucleation chamber that improves on common limitations from previous generations. The instrument is transportable, can be used as either a CCN or IN counter, covers a wide range of tropospheric conditions and shows a background signal significantly lower than previous generations. Finally, experimental evaluation of the instrument has revealed the presence of a potential bias in the way ice nucleation data is currently treated within the community. This finding may change the conventional way in which ice nucleation results are analyzed.

ACKNOWLEDGEMENTS

Erik - Thank you for giving me the opportunity to spend these years working in the Atmospheric Science group. It has not always been easy but it was good to know that I could always get your help whenever I needed it and that you always remained calm and logical to get through situations. I have learnt a lot through these 5 years thanks to your guidance, and I owe you some important life lessons that I will keep in mind for the rest of my life.

Kong - Thank you for your full support whenever I needed guidance and thank you for reaching out whenever you thought I may need guidance. Those night shifts in PSI could have felt much longer than they did if it was not for the good humor and the japanese series. I wish you all the best for the future and I hope we remain in touch :).

Mattias, Johan and Jan - Thank you for making the Atmospheric Science division such a nice place to work in. Thanks for all the fikas, liseberg, bowling, restaurant events. You have always prioritized a good atmosphere in the division and it was truly a pleasure to work with you.

Sofia and Sam - Big sis, big bro, thanks for taking me under your wing when I first arrived into the group. Thanks for being the best office mates and my best friends. I truly missed you both when you left the group, the dirty humor has never been to the same level after that. Nondas is trying to keep it going but it feels like something is missing. I have decided to stay a while longer in Sweden and I promise to be better at staying in touch. I love you both. ♥

Zoé, Yusheng and Jonathan - Yusheng, thanks for the help provided developing PINCii, thank you for helping me debug the software and go through the madness of organizing thermocouples. Zoé, thanks for your involvement in PINCii's development and thanks for making the HyICE campaign a fun time. Jonathan, thank you for always keeping the positive attitude and keeping us motivated even when things explode and every hope seems to have disappeared.

Atmospheric Science Group - Thanks for the constant good atmosphere in the office and the chill attitude. Thanks for always be ready to help and share a coffee. It was really fun to work with everybody. I will miss you all and I hope you will all do awesome in the future.

Famille - Merci de m'avoir permis d'arriver jusqu'ici et merci de continuer à me soutenir malgrès mon abscence. Je vous aime.

Friends - Although you may not know much about my work and probably won't read this (please don't read this), I want to thank you for all the love and support, that's a big part of

what has been keeping me sane. Special thanks to Fathi Hussein for helping me translating the abstract to swedish.
Hanna - Thank you for spending so much time on the cover figure and the Hyytiälä figure. Thank you for always being by my side, ready to cheer me up when I need it and ready to kick my ass when I am procrastinating. Knowing that I would come home to you is probably the only thing that kept me sane in some situations. Thanks for being the best. Thanks for being you. I love you ♥

BIBLIOGRAPHY

[1] J. P. Abbatt, W. R. Leaitch, A. A. Aliabadi, A. K. Bertram, J.-P. Blanchet, A. Boivin-Rioux, H. Bozem, J. Burkart, R. Y. Chang, J. Charette, et al. Overview paper: New insights into aerosol and climate in the Arctic. *Atmospheric Chemistry and Physics*, 19(4):2527–2560, 2019.

[2] H. J. Aufm Kampe and H. K. Weickmann. The effectiveness of natural and artificial aerosols as freezing nuclei. *Journal of Atmospheric Sciences*, 8(5):283–288, 1951.

[3] S. Augustin, H. Wex, D. Niedermeier, B. Pummer, H. Grothe, S. Hartmann, L. Tomsche, T. Clauss, J. Voigtländer, K. Ignatius, et al. Immersion freezing of birch pollen washing water. *Atmospheric Chemistry and Physics*, 13(21):10989–11003, 2013.

[4] A. P. Ault and J. L. Axson. Atmospheric aerosol chemistry: Spectroscopic and microscopic advances. *Analytical Chemistry*, 89(1):430–452, 2017.

[5] R. Bahadur and L. M. Russell. Effect of surface tension from MD simulations on size-dependent deliquescence of NaCl nanoparticles. *Aerosol Science and Technology*, 42(5):369–376, 2008.

[6] T. Bergeron. On the physics of clouds and precipitation. *Proc. 5th Assembly UGGI, Lisbon, Portugal, 1935*, pages 156–180, 1935.

[7] G. Biskos, L. Russell, P. Buseck, and S. T. Martin. Nanosize effect on the hygroscopic growth factor of aerosol particles. *Geophysical Research Letters*, 33(7), 2006.

[8] O. Boucher, D. Randall, P. Artaxo, C. Bretherton, G. Feingold, P. Forster, V.-M. Kerminen, Y. Kondo, H. Liao, U. Lohmann, et al. Clouds and aerosols. In *Climate change 2013: the physical science basis. Contribution of Working Group I to the Fifth Assessment Report of the Intergovernmental Panel on Climate Change*, pages 571–657. Cambridge University Press, 2013.

[9] M. Boy, E. S. Thomson, J.-C. Acosta Navarro, O. Arnalds, E. Batchvarova, J. Bäck, F. Berninger, M. Bilde, Z. Brasseur, P. Dagsson-Waldhauserova, et al. Interactions between the atmosphere, cryosphere, and ecosystems at northern high latitudes. *Atmospheric Chemistry and Physics*, 19(3):2015–2061, 2019.

[10] Z. Brasseur, D. Castarède, E. S. Thomson, M. P. Adams, S. Drossaart van Dusseldorp, P. Heikkilä, K. Korhonen, J. Lampilahti, M. Paramonov, J. Schneider, et al. Measurement report: Introduction to the HyICE-2018 campaign for measurements of ice nucleating particles in the Hyytiälä boreal forest. *Atmospheric Chemistry and Physics Discussions*, pages 1–46, 2021.

[11] C. Brunner and Z. A. Kanji. Continuous online monitoring of ice-nucleating particles: development of the automated Horizontal Ice Nucleation Chamber (HINC-Auto). *Atmospheric Measurement Techniques*, 14(1):269–293, 2021.

[12] D. A. Bruzewicz, A. Checco, B. M. Ocko, E. R. Lewis, R. L. McGraw, and S. E. Schwartz. Reversible uptake of water on NaCl nanoparticles at relative humidity below deliquescence point observed by noncontact environmental atomic force microscopy. *The Journal of Chemical Physics*, 134(4):044702, 2011.

[13] J. B. Burkholder, R. Cox, and A. Ravishankara. Atmospheric degradation of ozone depleting substances, their substitutes, and related species. *Chemical Reviews*, 115 (10):3704–3759, 2015.

[14] D. Castarède and E. S. Thomson. A thermodynamic description for the hygroscopic growth of atmospheric aerosol particles. *Atmospheric Chemistry and Physics*, 18 (20):14939–14948, 2018.

[15] A. Chebbi and P. Carlier. Carboxylic acids in the troposphere, occurrence, sources, and sinks: A review. *Atmospheric Environment*, 30(24):4233–4249, 1996.

[16] J. Chen, X. Pei, H. Wang, J. Chen, Y. Zhu, M. Tang, and Z. Wu. Development, characterization, and validation of a cold stage-based ice nucleation array (PKU-INA). *Atmosphere*, 9(9):357, 2018.

[17] J.-C. Chen, B. Reischl, P. Spijker, N. Holmberg, K. Laasonen, and A. S. Foster. Ab initio kinetic monte carlo simulations of dissolution at the NaCl–water interface. *Physical Chemistry Chemical Physics*, 16(41):22545–22554, 2014.

[18] Y. Cheng, H. Su, T. Koop, E. Mikhailov, and U. Pöschl. Size dependence of phase transitions in aerosol nanoparticles. *Nature Communications*, 6(1):1–7, 2015.

[19] C. Chou. Investigation of ice nucleation properties onto soot, bioaerosol and mineral dust during different measurement campaigns. *PhD thesis, ETH Zurich*, 2011.

[20] É. Clapeyron. Mémoire sur la puissance motrice de la chaleur. *Journal de l'École Polytechnique*, 14:153–190, 1834.

[21] R. Clausius. Ueber die bewegende kraft der wärme und die gesetze, welche sich daraus für die wärmelehre selbst ableiten lassen. *Annalen der Physik*, 155(3):368–397, 1850.

[22] S. L. Clegg, P. Brimblecombe, and A. S. Wexler. Thermodynamic model of the system H^+- NH4$^+$ - SO_4^{2-} - NO_3^- - H_2O at tropospheric temperatures. *The Journal of Physical Chemistry A*, 102(12):2137–2154, 1998.

[23] F. Conen, S. Henne, C. E. Morris, and C. Alewell. Atmospheric ice nucleators active $\geq -12°$C can be quantified on PM 10 filters. *Atmospheric Measurement Techniques*, 5(2):321–327, 2012.

[24] J. A. Curry. Interactions among turbulence, radiation and microphysics in Arctic stratus clouds. *Journal of Atmospheric Sciences*, 43(1):90–106, 1986.

[25] M. Dal Maso, M. Kulmala, I. Riipinen, R. Wagner, T. Hussein, P. P. Aalto, and K. E. Lehtinen. Formation and growth of fresh atmospheric aerosols: eight years of aerosol size distribution data from SMEAR II, Hyytiala, Finland. *Boreal Environment Research*, 10(5):323, 2005.

[26] J. Dash, A. Rempel, and J. Wettlaufer. The physics of premelted ice and its geophysical consequences. *Reviews of Modern Physics*, 78(3):695, 2006.

[27] R. O. David, C. Marcolli, J. Fahrni, Y. Qiu, Y. A. P. Sirkin, V. Molinero, F. Mahrt, D. Brühwiler, U. Lohmann, and Z. A. Kanji. Pore condensation and freezing is responsible for ice formation below water saturation for porous particles. *Proceedings of the National Academy of Sciences*, 116(17):8184–8189, 2019.

[28] R. D. Davis, S. Lance, J. A. Gordon, S. B. Ushijima, and M. A. Tolbert. Contact efflorescence as a pathway for crystallization of atmospherically relevant particles. *Proceedings of the National Academy of Sciences*, 112(52):15815–15820, 2015.

[29] P. J. DeMott, A. J. Prenni, X. Liu, S. M. Kreidenweis, M. D. Petters, C. H. Twohy, M. Richardson, T. Eidhammer, and D. Rogers. Predicting global atmospheric ice nuclei distributions and their impacts on climate. *Proceedings of the National Academy of Sciences*, 107(25):11217–11222, 2010.

[30] R. Eastman and S. G. Warren. A 39-yr survey of cloud changes from land stations worldwide 1971–2009: Long-term trends, relation to aerosols, and expansion of the tropical belt. *Journal of Climate*, 26(4):1286–1303, 2013.

[31] G. E. Ewing. H_2O on NaCl: From single molecule, to clusters, to monolayer, to thin film, to deliquescence. *Intermolecular Forces and Clusters II, Springer*, pages 1–25, Berlin, Heidelberg, 2005.

[32] J. Fan, Y. Wang, D. Rosenfeld, and X. Liu. Review of aerosol–cloud interactions: Mechanisms, significance, and challenges. *Journal of the Atmospheric Sciences*, 73 (11):4221–4252, 2016.

[33] D. K. Farmer, C. D. Cappa, and S. M. Kreidenweis. Atmospheric processes and their controlling influence on cloud condensation nuclei activity. *Chemical Reviews*, 115 (10):4199–4217, 2015.

[34] F. Fdz-Polanco, M. Fdz-Polanco, N. Fernandez, M. Urueña, P. Garcia, and S. Villaverde. Combining the biological nitrogen and sulfur cycles in anaerobic conditions. *Water Science and Technology*, 44(8):77–84, 2001.

[35] P. R. Field, R. P. Lawson, P. R. Brown, G. Lloyd, C. Westbrook, D. Moisseev, A. Miltenberger, A. Nenes, A. Blyth, T. Choularton, et al. Secondary ice production: Current state of the science and recommendations for the future. *Meteorological Monographs*, 58:7–1, 2017.

[36] W. Findeisen. Kolloid-meteorologische vorgänge bei neiderschlags-bildung. *Meteorologische Zeitschrift*, 55:121–133, 1938.

[37] R. H. French. Origins and applications of london dispersion forces and hamaker constants in ceramics. *Journal of the American Ceramic Society*, 83(9):2117–2146, 2000.

[38] R. H. French, V. A. Parsegian, R. Podgornik, R. F. Rajter, A. Jagota, J. Luo, D. Asthagiri, M. K. Chaudhury, Y.-m. Chiang, S. Granick, et al. Long range interactions in nanoscale science. *Reviews of Modern Physics*, 82(2):1887, 2010.

[39] S. Garimella, T. B. Kristensen, K. Ignatius, A. Welti, J. Voigtländer, G. R. Kulkarni, F. Sagan, G. L. Kok, J. Dorsey, L. Nichman, et al. The SPectrometer for Ice Nuclei (SPIN): an instrument to investigate ice nucleation. *Atmospheric Measurement Techniques*, 9(7):2781–2795, 2016.

[40] C. George, M. Ammann, B. D'Anna, D. Donaldson, and S. A. Nizkorodov. Heterogeneous photochemistry in the atmosphere. *Chemical Reviews*, 115(10):4218–4258, 2015.

[41] M. Hallquist, J. C. Wenger, U. Baltensperger, Y. Rudich, D. Simpson, M. Claeys, J. Dommen, N. Donahue, C. George, A. Goldstein, et al. The formation, properties and impact of secondary organic aerosol: current and emerging issues. *Atmospheric Chemistry and Physics*, 9(14):5155–5236, 2009.

[42] G. Halsey. Physical adsorption on non-uniform surfaces. *The Journal of Chemical Physics*, 16(10):931–937, 1948.

[43] K. Hämeri, A. Laaksonen, M. Väkevä, and T. Suni. Hygroscopic growth of ultrafine sodium chloride particles. *Journal of Geophysical Research: Atmospheres*, 106 (D18):20749–20757, 2001.

[44] H. Hansen-Goos, E. S. Thomson, and J. Wettlaufer. On the edge of habitability and the extremes of liquidity. *Planetary and Space Science*, 98:169–181, 2014.

[45] P. Hari, E. Nikinmaa, T. Pohja, E. Siivola, J. Bäck, T. Vesala, and M. Kulmala. Station for measuring ecosystem-atmosphere relations: SMEAR. In *Physical and Physiological Forest Ecology*, pages 471–487. Springer, 2013.

[46] J. Y. Harrington, T. Reisin, W. R. Cotton, and S. M. Kreidenweis. Cloud resolving simulations of Arctic stratus: Part II: Transition-season clouds. *Atmospheric Research*, 51(1):45–75, 1999.

[47] W. M. Haynes. CRC Handbook of chemistry and physics. *CRC Press*, 2014.

[48] T. C. Hill, B. F. Moffett, P. J. DeMott, D. G. Georgakopoulos, W. L. Stump, and G. D. Franc. Measurement of ice nucleation-active bacteria on plants and in precipitation by quantitative PCR. *Applied and Environmental Microbiology*, 80(4):1256–1267, 2014.

[49] T. L. Hill. Physical adsorption and the free volume model for liquids. *The Journal of Chemical Physics*, 17(6):590–590, 1949.

[50] C. Hoose and O. Möhler. Heterogeneous ice nucleation on atmospheric aerosols: a review of results from laboratory experiments. *Atmospheric Chemistry and Physics*, 12(20):9817–9854, 2012.

[51] L. Howard. On the modifications of clouds, and on the principles of their production, suspension, and destruction. *The Philosophical Magazine*, 17(65):5–11, 1803.

[52] R.-J. Huang, Y. Zhang, C. Bozzetti, K.-F. Ho, J.-J. Cao, Y. Han, K. R. Daellenbach, J. G. Slowik, S. M. Platt, F. Canonaco, et al. High secondary aerosol contribution to particulate pollution during haze events in china. *Nature*, 514(7521):218–222, 2014.

[53] K. Hussain and C. P. Saunders. Ice nucleus measurement with a continuous flow chamber. *Quarterly Journal of the Royal Meteorological Society*, 110(463):75–84, 1984.

[54] H. Jiang, W. R. Cotton, J. O. Pinto, J. A. Curry, and M. J. Weissbluth. Cloud resolving simulations of mixed-phase Arctic stratus observed during BASE: Sensitivity to concentration of ice crystals and large-scale heat and moisture advection. *Journal of the Atmospheric Sciences*, 57(13):2105–2117, 2000.

[55] Z. A. Kanji and J. P. Abbatt. The University of Toronto continuous flow diffusion chamber (UT-CFDC): A simple design for ice nucleation studies. *Aerosol Science and Technology*, 43(7):730–738, 2009.

[56] Z. A. Kanji, L. A. Ladino, H. Wex, Y. Boose, M. Burkert-Kohn, D. J. Cziczo, and M. Krämer. Overview of ice nucleating particles. *Meteorological Monographs*, 58: 1–1, 2017.

[57] K. Kawamura, L. L. Ng, and I. R. Kaplan. Determination of organic acids (C1-C10) in the atmosphere, motor exhausts, and engine oils. *Environmental Science & Technology*, 19(11):1082–1086, 1985.

[58] J. Kesselmeier and M. Staudt. Biogenic volatile organic compounds (VOC): an overview on emission, physiology and ecology. *Journal of Atmospheric Chemistry*, 33(1):23–88, 1999.

[59] A. Kiselev, F. Bachmann, P. Pedevilla, S. J. Cox, A. Michaelides, D. Gerthsen, and T. Leisner. Active sites in heterogeneous ice nucleation—the example of K-rich feldspars. *Science*, 355(6323):367–371, 2017.

[60] K. Kobayashi, Y. Liang, T. Sakka, and T. Matsuoka. Molecular dynamics study of salt–solution interface: Solubility and surface charge of salt in water. *The Journal of Chemical Physics*, 140(14):144705, 2014.

[61] H. Köhler. The nucleus in and the growth of hygroscopic droplets. *Transactions of the Faraday Society*, 32:1152–1161, 1936.

[62] X. Kong, D. Castarède, A. Boucly, L. Artiglia, M. Ammann, T. Bartels-Rausch, E. S. Thomson, and J. B. Pettersson. Reversibly physisorbed and chemisorbed water on carboxylic salt surfaces under atmospheric conditions. *The Journal of Physical Chemistry C*, 124(9):5263–5269, 2020.

[63] X. Kong, D. Castarède, E. S. Thomson, A. Boucly, L. Artiglia, M. Ammann, I. Gladich, and J. B. C. Pettersson. A surface-promoted redox reaction occurs spontaneously on solvating inorganic aerosol surfaces. *Science*, 374(6568):747–752, 2021.

[64] T. Koop, B. Luo, A. Tsias, and T. Peter. Water activity as the determinant for homogeneous ice nucleation in aqueous solutions. *Nature*, 406(6796):611–614, 2000.

[65] A. Korolev. Limitations of the Wegener–Bergeron–Findeisen mechanism in the evolution of mixed-phase clouds. *Journal of the Atmospheric Sciences*, 64(9):3372–3375, 2007.

[66] A. V. Korolev and I. P. Mazin. Supersaturation of water vapor in clouds. *Journal of Atmospheric Sciences*, 60(24):2957–2974, 2003.

[67] A. Laaksonen. A unifying model for adsorption and nucleation of vapors on solid surfaces. *The Journal of Physical Chemistry A*, 119(16):3736–3745, 2015.

[68] L. Lacher, U. Lohmann, Y. Boose, A. Zipori, E. Herrmann, N. Bukowiecki, M. Steinbacher, and Z. A. Kanji. The Horizontal Ice Nucleation Chamber (HINC): INP measurements at conditions relevant for mixed-phase clouds at the High Altitude Research Station Jungfraujoch. *Atmospheric Chemistry and Physics*, 17(24):15199–15224, 2017.

[69] G. Langer and J. Rodgers. An experimental study of the detection of ice nuclei on membrane filters and other substrata. *Journal of Applied Meteorology and Climatology*, 14(4):560–570, 1975.

[70] O. Laskina, H. S. Morris, J. R. Grandquist, Z. Qin, E. A. Stone, A. V. Tivanski, and V. H. Grassian. Size matters in the water uptake and hygroscopic growth of atmospherically relevant multicomponent aerosol particles. *The Journal of Physical Chemistry A*, 119(19):4489–4497, 2015.

[71] E. R. Lewis and S. E. Schwartz. Sea salt aerosol production: mechanisms, methods, measurements, and models. *American Geophysical Union*, Washington DC, 2004.

[72] L.-M. Liu, A. Laio, and A. Michaelides. Initial stages of salt crystal dissolution determined with ab initio molecular dynamics. *Physical Chemistry Chemical Physics*, 13(29):13162–13166, 2011.

[73] U. Lohmann and J. Feichter. Global indirect aerosol effects: a review. *Atmospheric Chemistry and Physics*, 5(3):715–737, 2005.

[74] U. Lohmann, F. Lüönd, and F. Mahrt. An introduction to clouds: From the microscale to climate. *Cambridge University Press*, Cambridge, 2016.

[75] Q. Ma, Y. Liu, and H. He. The utilization of physisorption analyzer for studying the hygroscopic properties of atmospheric relevant particles. *The Journal of Physical Chemistry A*, 114(12):4232–4237, 2010.

[76] F. Mahrt. A burning issue-Soot particles acting as ice cloud seeds. *PhD thesis, ETH Zurich*, 2019.

[77] C. Marcolli. Fundamental aspects of ice nucleation via pore condensation and freezing including laplace pressure and growth into macroscopic ice. *Atmospheric Chemistry and Physics*, 20(5):3209–3230, 2020.

[78] S. T. Martin. Phase transitions of aqueous atmospheric particles. *Chemical Reviews*, 100(9):3403–3454, 2000.

[79] B. J. Mason. The cloud chamber as a tool in cloud physics. *Contemporary Physics*, 4(1):27–48, 1962.

[80] E. Mikhailov, S. Vlasenko, D. Rose, and U. Pöschl. Mass-based hygroscopicity parameter interaction model and measurement of atmospheric aerosol water uptake. *Atmospheric Chemistry and Physics*, 13(2):717–740, 2013.

[81] Y. Ming and L. M. Russell. Predicted hygroscopic growth of sea salt aerosol. *Journal of Geophysical Research: Atmospheres*, 106(D22):28259–28274, 2001.

[82] O. Möhler, M. Adams, L. Lacher, F. Vogel, J. Nadolny, R. Ullrich, C. Boffo, T. Pfeuffer, A. Hobl, M. Weiß, et al. The Portable Ice Nucleation Experiment (PINE): a new online instrument for laboratory studies and automated long-term field observations of ice-nucleating particles. *Atmospheric Measurement Techniques*, 14(2):1143–1166, 2021.

[83] C. E. Morris, F. Conen, J. Alex Huffman, V. Phillips, U. Pöschl, and D. C. Sands. Bioprecipitation: a feedback cycle linking earth history, ecosystem dynamics and land use through biological ice nucleators in the atmosphere. *Global Change Biology*, 20(2):341–351, 2014.

[84] H. Morrison, G. De Boer, G. Feingold, J. Harrington, M. D. Shupe, and K. Sulia. Resilience of persistent Arctic mixed-phase clouds. *Nature Geoscience*, 5(1):11–17, 2012.

[85] S. Mossop and A. Ono. Measurements of ice crystal concentration in clouds. *Journal of Atmospheric Sciences*, 26(1):130–137, 1969.

[86] B. Murray, S. Broadley, T. Wilson, S. Bull, R. Wills, H. Christenson, and E. Murray. Kinetics of the homogeneous freezing of water. *Physical Chemistry Chemical Physics*, 12(35):10380–10387, 2010.

[87] M. Nicolet, O. Stetzer, F. Lüönd, O. Möhler, and U. Lohmann. Single ice crystal measurements during nucleation experiments with the depolarization detector IODE. *Atmospheric Chemistry and Physics*, 10(2):313–325, 2010.

[88] F. Orlando, A. Waldner, T. Bartels-Rausch, M. Birrer, S. Kato, M.-T. Lee, C. Proff, T. Huthwelker, A. Kleibert, J. Van Bokhoven, et al. The environmental photochemistry of oxide surfaces and the nature of frozen salt solutions: a new in situ XPS approach. *Topics in Catalysis*, 59(5-7):591–604, 2016.

[89] N. Ottosson, E. Wernersson, J. Söderström, W. Pokapanich, S. Kaufmann, S. Svensson, I. Persson, G. Öhrwall, and O. Björneholm. The protonation state of small carboxylic acids at the water surface from photoelectron spectroscopy. *Physical Chemistry Chemical Physics*, 13(26):12261–12267, 2011.

[90] M. Paramonov, S. Drossaart van Dusseldorp, E. Gute, J. P. Abbatt, P. Heikkilä, J. Keskinen, X. Chen, K. Luoma, L. Heikkinen, L. Hao, et al. Condensation/immersion mode ice-nucleating particles in a boreal environment. *Atmospheric Chemistry and Physics*, 20(11):6687–6706, 2020.

[91] S. J. Peters and G. E. Ewing. Thin film water on NaCl (100) under ambient conditions: An infrared study. *Langmuir*, 13(24):6345–6348, 1997.

[92] J. O. Pinto. Autumnal mixed-phase cloudy boundary layers in the Arctic. *Journal of the Atmospheric Sciences*, 55(11):2016–2038, 1998.

[93] G. C. Porter, S. N. Sikora, M. P. Adams, U. Proske, A. D. Harrison, M. D. Tarn, I. M. Brooks, and B. J. Murray. Resolving the size of ice-nucleating particles with a balloon deployable aerosol sampler: the SHARK. *Atmospheric Measurement Techniques*, 13(6):2905–2921, 2020.

[94] U. Pöschl. Atmospheric aerosols: composition, transformation, climate and health effects. *Angewandte Chemie International Edition*, 44(46):7520–7540, 2005.

[95] K. A. Prather, C. D. Hatch, and V. H. Grassian. Analysis of atmospheric aerosols. *Annual Review of Analytical Chemistry*, 1:485–514, 2008.

[96] B. G. Pummer, H. Bauer, J. Bernardi, S. Bleicher, and H. Grothe. Suspendable macromolecules are responsible for ice nucleation activity of birch and conifer pollen. *Atmospheric Chemistry and Physics*, 12(5):2541–2550, 2012.

[97] A. L. Rangno and P. V. Hobbs. Ice particles in stratiform clouds in the Arctic and possible mechanisms for the production of high ice concentrations. *Journal of Geophysical Research: Atmospheres*, 106(D14):15065–15075, 2001.

[98] F.-M. Raoult. Loi générale des tensions de vapeur des dissolvants. *Comptes rendus hebdomadaires des séances de l'Académie des Sciences.*, 104:1430–1433, 1887.

[99] E. Rikmann, I. Zekker, M. Tomingas, T. Tenno, A. Menert, L. Loorits, and T. Tenno. Sulfate-reducing anaerobic ammonium oxidation as a potential treatment method for high nitrogen-content wastewater. *Biodegradation*, 23(4):509–524, 2012.

[100] D. C. Rogers. Development of a continuous flow thermal gradient diffusion chamber for ice nucleation studies. *Atmospheric Research*, 22(2):149–181, 1988.

[101] M. J. Rossi. Heterogeneous reactions on salts. *Chemical Reviews*, 103(12):4823–4882, 2003.

[102] L. M. Russell and Y. Ming. Deliquescence of small particles. *The Journal of Chemical Physics*, 116(1):311–321, 2002.

[103] T. Schiebel. Ice nucleation activity of soil dust aerosols. *PhD thesis, KIT-Bibliothek*, 2017.

[104] J. Schneider, K. Höhler, P. Heikkilä, J. Keskinen, B. Bertozzi, P. Bogert, T. Schorr, N. S. Umo, F. Vogel, Z. Brasseur, et al. The seasonal cycle of ice-nucleating particles linked to the abundance of biogenic aerosol in boreal forests. *Atmospheric Chemistry and Physics*, 21(5):3899–3918, 2021.

[105] J. Schneider, K. Höhler, R. Wagner, H. Saathoff, M. Schnaiter, T. Schorr, I. Steinke, S. Benz, M. Baumgartner, C. Rolf, et al. High homogeneous freezing onsets of sulfuric acid aerosol at cirrus temperatures. *Atmospheric Chemistry and Physics Discussions*, pages 1–30, 2021.

[106] J. Schrod, A. Danielczok, D. Weber, M. Ebert, E. S. Thomson, and H. G. Bingemer. Re-evaluating the Frankfurt isothermal static diffusion chamber for ice nucleation. *Atmospheric Measurement Techniques*, 9(3):1313–1324, 2016.

[107] J. Sedlar and M. Tjernström. Stratiform cloud—inversion characterization during the Arctic melt season. *Boundary-Layer Meteorology*, 132(3):455–474, 2009.

[108] M. Shiraiwa, K. Ueda, A. Pozzer, G. Lammel, C. J. Kampf, A. Fushimi, S. Enami, A. M. Arangio, J. Frohlich-Nowoisky, Y. Fujitani, et al. Aerosol health effects from molecular to global scales. *Environmental Science & Technology*, 51(23):13545–13567, 2017.

[109] M. D. Shupe. Clouds at Arctic atmospheric observatories. Part II: Thermodynamic phase characteristics. *Journal of Applied Meteorology and Climatology*, 50(3):645–661, 2011.

[110] A. Sinnarwalla and D. Alofs. A cloud nucleus counter with long available growth time. *Journal of Applied Meteorology*, 12(5):831–835, 1973.

[111] A. Solomon, M. D. Shupe, P. Persson, and H. Morrison. Moisture and dynamical interactions maintaining decoupled Arctic mixed-phase stratocumulus in the presence of a humidity inversion. *Atmospheric Chemistry and Physics*, 11(19):10127–10148, 2011.

[112] O. Stetzer, B. Baschek, F. Lüönd, and U. Lohmann. The Zurich Ice Nucleation Chamber (ZINC)-A new instrument to investigate atmospheric ice formation. *Aerosol Science and Technology*, 42(1):64–74, 2008.

[113] R. Stokes and R. Robinson. Interactions in aqueous nonelectrolyte solutions. I. Solute-solvent equilibria. *The Journal of Physical Chemistry*, 70(7):2126–2131, 1966.

[114] E. Stopelli, F. Conen, L. Zimmermann, C. Alewell, and C. E. Morris. Freezing nucleation apparatus puts new slant on study of biological ice nucleators in precipitation. *Atmospheric Measurement Techniques*, 7(1):129–134, 2014.

[115] T. Storelvmo, J. E. Kristjánsson, and U. Lohmann. Aerosol influence on mixed-phase clouds in CAM-Oslo. *Journal of the Atmospheric Sciences*, 65(10):3214–3230, 2008.

[116] C. J. Stubenrauch, W. B. Rossow, S. Kinne, S. Ackerman, G. Cesana, H. Chepfer, L. Di Girolamo, B. Getzewich, A. Guignard, A. Heidinger, et al. Assessment of global cloud datasets from satellites: Project and database initiated by the GEWEX radiation panel. *Bulletin of the American Meteorological Society*, 94(7):1031–1049, 2013.

[117] J.-B. W. Stuut et al. Mineral dust: A key player in the earth system. *Springer*, 2014.

[118] R. W. Talbot, B. W. Mosher, B. G. Heikes, D. J. Jacob, J. W. Munger, B. C. Daube, W. C. Keene, J. R. Maben, and R. S. Artz. Carboxylic acids in the rural continental atmosphere over the eastern united states during the Shenandoah Cloud and Photochemistry Experiment. *Journal of Geophysical Research: Atmospheres*, 100(D5): 9335–9343, 1995.

[119] I. N. Tang, A. Tridico, and K. Fung. Thermodynamic and optical properties of sea salt aerosols. *Journal of Geophysical Research: Atmospheres*, 102(D19):23269–23275, 1997.

[120] P. Tunved, H.-C. Hansson, V.-M. Kerminen, J. Ström, M. Dal Maso, H. Lihavainen, Y. Viisanen, P. P. Aalto, M. Komppula, and M. Kulmala. High natural aerosol loading over boreal forests. *Science*, 312(5771):261–263, 2006.

[121] S. B. Ushijima, R. D. Davis, and M. A. Tolbert. Immersion and contact efflorescence induced by mineral dust particles. *The Journal of Physical Chemistry A*, 122(5): 1303–1311, 2018.

[122] G. Vali, P. J. DeMott, O. Möhler, and T. F. Whale. A proposal for ice nucleation terminology. *Atmospheric Chemistry and Physics*, 15(18):10263–10270, 2015.

[123] A. Verdaguer, G. Sacha, M. Luna, D. Frank Ogletree, and M. Salmeron. Initial stages of water adsorption on NaCl (100) studied by scanning polarization force microscopy. *The Journal of Chemical Physics*, 123(12):124703, 2005.

[124] J. Verlinde, J. Y. Harrington, G. McFarquhar, V. Yannuzzi, A. Avramov, S. Greenberg, N. Johnson, G. Zhang, M. Poellot, J. H. Mather, et al. The mixed-phase Arctic cloud experiment. *Bulletin of the American Meteorological Society*, 88(2):205–222, 2007.

[125] B. Vonnegut. The nucleation of ice formation by silver iodide. *Journal of Applied Physics*, 18(7):593–595, 1947.

[126] A. Wegener. Thermodynamik der atmosphäre. *JA Barth*, 1911.

[127] A. Welti, K. Korhonen, P. Miettinen, A. A. Piedehierro, Y. Viisanen, A. Virtanen, and A. Laaksonen. SPIN modification for low-temperature experiments. *Atmospheric Measurement Techniques*, 13(12):7059–7067, 2020.

[128] C. T. Wilson. Condensation of water vapour in the presence of dust-free air and other gases. *Philosophical Transactions of the Royal Society of London. Series A, Containing Papers of a Mathematical or Physical Character*, (189):265–307, 1897.

[129] M. E. Wise, S. T. Martin, L. M. Russell, and P. R. Buseck. Water uptake by NaCl particles prior to deliquescence and the phase rule. *Aerosol Science and Technology*, 42(4):281–294, 2008.

[130] M. E. Wise, E. J. Freney, C. A. Tyree, J. O. Allen, S. T. Martin, L. M. Russell, and P. R. Buseck. Hygroscopic behavior and liquid-layer composition of aerosol particles generated from natural and artificial seawater. *Journal of Geophysical Research: Atmospheres*, 114(D3), 2009.

[131] D. Wylie, D. L. Jackson, W. P. Menzel, and J. J. Bates. Trends in global cloud cover in two decades of HIRS observations. *Journal of Climate*, 18(15):3021–3031, 2005.

[132] B. E. Wyslouzil and J. Wölk. Overview: Homogeneous nucleation from the vapor phase—the experimental science. *The Journal of Chemical Physics*, 145(21):211702, 2016.

[133] J.-I. Yano and V. Phillips. Ice–ice collisions: An ice multiplication process in atmospheric clouds. *Journal of the Atmospheric Sciences*, 68(2):322–333, 2011.

[134] A. Zuend, C. Marcolli, B. P. Luo, and T. Peter. A thermodynamic model of mixed organic-inorganic aerosols to predict activity coefficients. *Atmospheric Chemistry and Physics*, 8(16):4559–4593, 2008.

[135] P. Zuidema, B. Baker, Y. Han, J. Intrieri, J. Key, P. Lawson, S. Matrosov, M. Shupe, R. Stone, and T. Uttal. An Arctic springtime mixed-phase cloudy boundary layer observed during SHEBA. *Journal of the Atmospheric Sciences*, 62(1):160–176, 2005.